CNWRA *A center of excellence in earth sciences and engineering*

A Division of Southwest Research Institute®
6220 Culebra Road • San Antonio, Texas, U.S.A. 78228-5166
(210) 522-5160 • Fax (210) 522-5155

September 8, 2005
Contract No. NRC–02–02–012
Account No. 20.06002.01.342

U.S. Nuclear Regulatory Commission
Attn: Dr. Mysore S. Nataraja
Division of High-Level Waste Repository Safety
Two White Flint North
11545 Rockville Pike
Mail Stop T–7F3
Washington, DC 20555

SUBJECT: Submission of Intermediate Milestone 20.06002.01.342.510, New and Revised MECHFAIL Total-system Performance Assessment Module Abstractions

Dear Dr. Nataraja:

Attached is the Center for Nuclear Waste Regulatory Analyses document "Structural Performance of Drip Shield Subjected to Static and Dynamic Loading." To better reflect the content of this report, the title has been changed from that in the fiscal year 2005 Operations Plan. This document fulfills the requirements for the subject milestone, which is due September 9, 2005.

This study calculates the structural response of the drip shield subjected to static and dynamic loading. The drip shield structure is modeled using both an ABAQUS finite element model and an equivalent SAP2000 structural frame model. The frame model is used to calculate the structural response of the drip shield under several static loading conditions. Also, seismic analyses are performed by subjecting the drip shield frame model to nonlinear time history analyses. The results of this study will facilitate staff review of the U.S. Department of Energy potential license application in the area of mechanical disruption of engineered barriers. In addition, this study will contribute to the development of new abstractions for the Total-system Performance Assessment code module MECHFAIL.

The document transmitted herewith contains sensitive unclassified information.
When separated from enclosures, this document is decontrolled.

Washington Office • Twinbrook Metro Plaza #210
12300 Twinbrook Parkway • Rockville, Maryland 20852-1606

If you have any questions concerning this milestone, please contact me at (210) 522-5151 or Luis Ibarra at (210) 522-5152.

Sincerely,

Asadul H. Chowdhury, Manager
Mining, Geotechnical, and
Facility Engineering

AHC: ar

cc:

		Letter Only
B. Meehan	W. Patrick	L. Gutierrez
D. DeMarco	B. Sagar	CNWRA Directors
E. Whitt	S. Mohanty	CNWRA Managers
W. Reamer	A. Chowdhury	
W. Ford	A. Ghosh	
T. McCartin	S. Hsiung	
E. Collins	B. Dasgupta	
L. Kokajko	G. Ofoegbu	
A. Campbell	L. Ibarra	
T. Kobetz	T. Wilt	
Y. Kim	F. Ferrante	
M. Shah	Record Copy B, IQS	
B. Jagannath		
K. Stablein		
M. Bailey		
J. Guttmann		

The document transmitted herewith contains sensitive unclassified information.
When separated from enclosures, this document is decontrolled.

STRUCTURAL PERFORMANCE OF DRIP SHIELD SUBJECTED TO STATIC AND DYNAMIC LOADING

Prepared for

U.S. Nuclear Regulatory Commission
Contract NRC–02–02–012

Prepared by

L. Ibarra
T. Wilt
G. Ofoegbu
A. Chowdhury

Center for Nuclear Waste Regulatory Analyses
San Antonio, Texas

September 2005

LIMITED INTERNAL DISTRIBUTION PERMITTED

ABSTRACT

The U.S. Nuclear Regulatory Commission is interacting with the U.S. Department of Energy to gain insight into proposed engineered barriers design and related site characteristics associated with the potential geologic repository at Yucca Mountain, Nevada. In support of these pre-licensing interactions, this study independently investigates the static and dynamic structural performance of the proposed drip shield, an engineered barrier system included in the design of the potential geologic repository at the Yucca Mountain site in Nevada. The primary purpose of the drip shield is to limit the amount of water contacting the waste package as a result of seepage into the near-field environment. To accomplish this objective, the drip shield has to be able to withstand rockfall impacts, and static and dynamic loads resulting from the accumulated rockfall rubble. Drip shield structural instability would cause the drip shield and the waste package to interact, potentially triggering high localized plastic stresses in the waste package.

The drip shield structure is modeled using both an ABAQUS (ABAQUS, Inc., 2004) finite element model and an equivalent SAP2000 (Computers and Structures, Inc., 2004) frame model. The ABAQUS finite element model verifies the structural response obtained from the equivalent SAP2000 drip shield frame model. The finite element model also provides information about the moment-rotation relationships of the drip shield sections, and equivalent spring constants to account for drip shield-rubble interaction. The frame model is then used to evaluate the structural performance of the drip shield based on sensitivity studies and seismic analyses. The drip shield frame model results indicate that the most recent drip shield design cannot withstand the expected static and dynamic loads. The failure mode under static loads is plastic buckling of the drip shield columns for most of the evaluated loading configurations. When the drip shield strength capacity is sufficient to withstand the applied static loads, seismic events will very likely lead to structural collapse because the dynamic loads may be more than one order of magnitude larger than the static loads.

REFERENCES

ABAQUS, Inc. “ABAQUS User’s Manual.” Version 6.4. Providence, Rhode Island: ABAQUS, Inc. 2004.

Computers and Structures, Inc. “SAP2000 Version 8.3.1, Integrated Software for Structural Analysis and Design.” Berkeley, California. Computers and Structures, Inc. 2004.

CONTENTS

Section Page

ABSTRACT . . . iii
FIGURES . . . vii
TABLES . . . xi
ACKNOWLEDGMENTS . . . xiii

1 INTRODUCTION . . . 1-1
1.1 Background . . . 1-1
1.2 Objective and Scope . . . 1-2

2 DRIP SHIELD FINITE ELEMENT MODEL . . . 2-1
2.1 Introduction . . . 2-1
2.2 Description of Detailed ABAQUS Drip Shield Finite Element Model . . . 2-4
2.2.1 Material of Drip Shield Finite Element Model . . . 2-5
2.2.1.1 Drip Shield Material Properties . . . 2-5
2.2.1.2 Rockfall Rubble Material Properties . . . 2-9
2.2.2 Boundary Conditions . . . 2-12
2.2.2.1 Kinematic Constraints . . . 2-12
2.2.2.2 Loads . . . 2-12
2.3 Drip Shield Finite Element Models and Results . . . 2-13
2.3.1 Calculation of Spring Constants Using the Drip Shield Finite Element Model . . . 2-13
2.3.2 Moment-Rotation Curves . . . 2-15
2.3.2.1 Drip Shield Corner . . . 2-15
2.3.2.2 Drip Shield Support Beam . . . 2-17
2.3.3 Drip Shield Finite Element Models Used to Validate the Drip Shield Frame Model . . . 2-17

3 DRIP SHIELD FRAME MODEL . . . 3-1
3.1 Frame Model Description . . . 3-1
3.1.1 Frame Model Geometry . . . 3-1
3.1.2 Nonlinear Inelastic Rotational Springs . . . 3-5
3.1.3 Drip Shield Frame Model Material Properties . . . 3-7
3.1.3.1 Drip Shield Material Properties . . . 3-7
3.1.3.2 Rockfall Rubble Material Properties . . . 3-7
3.1.4 Frame Model Boundary Conditions . . . 3-7
3.1.4.1 Kinematic Constraints . . . 3-7
3.1.4.2 Static Loads . . . 3-8
3.2 Verification of the Drip Shield Frame Model Using a Drip Shield Finite Element Model . . . 3-12
3.2.1 Comparison of Displacements and Reactions . . . 3-13
3.2.2 Comparison of Ultimate Load Carrying Capacity . . . 3-13
3.3 SAP2000 Baseline Frame Model . . . 3-13
3.3.1 Drip Shield Response Under Normalized Loading Configuration . . . 3-16
3.3.2 Drip Shield Response Under Monotonically Increasing Loads Until the Onset of Structural Instability . . . 3-18

CONTENTS (continued)

Section Page

4 DRIP SHIELD SENSITIVITY ANALYSIS 4-1
4.1 Rubble Modulus of Elasticity Variation 4-1
4.2 Static Loading Variation 4-2
4.2.1 Lateral Loading Asymmetry Variation 4-4
4.2.2 Variation of Average Lateral-to-Vertical Load Ratios 4-6
4.3 Invert Degradation Variation 4-11
4.4 Temperature Variation 4-12
4.5 Effect of General Corrosion on Titanium Plates 4-14
4.6 Staged Loading 4-15

5 DRIP SHIELD SEISMIC ANALYSIS 5-1
5.1 Introduction 5-1
5.2 Frame Model Geometry 5-1
5.2.1 Nonlinear Inelastic Rotational Springs 5-1
5.2.2 Frame Model Viscous Damping 5-2
5.2.3 Drip Shield Frame Model Material Properties 5-2
5.2.3.1 Drip Shield Material Properties 5-2
5.2.3.2 Rockfall Rubble Material Properties 5-2
5.2.4 Frame Model Boundary Conditions 5-2
5.2.4.1 Kinematic Constraints 5-2
5.2.4.2 Static Loads 5-3
5.2.4.3 Dynamic Loads 5-3
5.3 Dynamic Time History Analysis for Records with Mean Annual Frequency of Exceedance of 1×10^{-5} 5-13

6 SUMMARY AND CONCLUSIONS 6-1
6.1 Summary 6-1
6.2 Static Loading 6-1
6.3 Seismic Loading 6-3
6.4 Uncertainty in the Drip Shield Frame Model 6-3
6.5 Conclusion 6-3

7 REFERENCES 7-1

APPENDICES

FIGURES

Figure Page

2-1 Illustration of the Engineered Barrier System Components Within the Emplacement Drift of the Potential Geologic Repository 2-2
2-2 (a) Isometric of Updated Drip Shield and (b) Drip Shield Crown Selection 2-3
2-3 Isometric of Drip Shield Finite Element Model 2-5
2-4 Drip Shield Finite Element Model with Uniform Normal Pressure 2-6
2-5 Drip Shield Corner Section 2-6
2-6 (a) Dependence of Yield Stress on Temperature, (b) Dependence of Ultimate Tensile Stress on Temperature, and (c) Dependence of Modulus of Elasticity (*E*) on Temperature 2-8
2-7 True Stress-Logarithmic Strain Curves for Titanium Grade 7 and Titanium Grade 24 at 24 at 150 °C [202 °F] 2-11
2-8 Drip Shield Finite Element Model for Obtaining Soil Spring Constants 2-14
2-9 Variation of Soil Springs Constants With Drip Shield Height 2-15
2-10 (a) Finite Element Model of the Drip Shield Corner to Obtain Moment-Rotation Curve (Interior View) and (b) Finite Element Model of the Drip Shield Corner to Obtain Moment-Rotation Curve (Exterior View) 2-16
2-11 Moment-Rotation Titanium Grade 7 Yield Stress at Failure (Internal View) 2-18
2-12 (a) Moment-Rotation Titanium Grade 24 Yield Stress at Failure (Internal View) and (b) Moment-Rotation Titanium Grade 24 Yield Stress at Failure (External View) . . 2-19
2-13 Moment-Rotation Curve for Drip Shield Corner 2-19
2-14 Analysis of Titanium Grade 24 Support Beam 2-20
2-15 Moment-Rotation Response at the Support Beam from Finite Element Model 2-20
2-16 Drip Shield Von Mises Stress Distribution of Titanium Grade 24 First Yield 2-21
2-17 Drip Shield Von Mises Stress Distribution at Failure 2-22

3-1 Discretization of Drip Shield Frame Model (a) Node Labels and (b) Element Labels 3-3
3-2 Cross Sections for Drip Shield Frame Model (a) Support Beam Columns and (b) Bulkhead (Beams) 3-4
3-3 Idealized Moment-Rotation Relationship of Drip Shield Cross Sections 3-6
3-4 Drip Shield Frame Model Kinematic Constraints 3-8
3-5 Uniform Distributed Drip Shield Loads for the Baseline Loading Case (KN/m). (a) Vertical Loads Projected to Drip Shield Crown and (b) Horizontal Loads Projected to Drip Wall and Crown 3-9
3-6 Vertical Load on the Drip Shield as a Function of the Bulking Factor 3-11
3-7 Comparison of Frame Model and Finite Element Model Vertical Load Carrying for Capacity for Critical Column Sections, Case I 3-15
3-8 Comparison of Frame Model and Finite Element Model Vertical Load Carrying Capacity for Critical Column Sections, Case II 3-15
3-9 Drip Shield Deformed Shape for “Normalized” Baseline Loading Pattern 3-17
3-10 Drip Shield Axial Forces for “Normalized” Baseline Loading Pattern 3-18
3-11 Drip Shield Bending Moments for “Normalized” Baseline Loading Pattern 3-19
3-12 Drip Shield Deformed Shape for Baseline Model Under Different Loading Levels (a) P_v = 188 KPa [27 psi], (b) P_v = 237 KPa [34 psi], (c) P_v = 290 KPa [42 psi], and (d) P_v = 298 KPa [43 psi] 3-20

FIGURES (continued)

Section Page

3-13 Vertical Load Carrying Capacity Versus Horizontal Displacement at Critical Column Sections for Baseline Loading Pattern 3-21

4-1 Effect of Rubble Modulus of Elasticity on the Drip Shield Bending Moment Diagrams at the Onset of Structural Instability, (a) E_r = 0 MPa and (b) E_r = 100 MPa 4-3
4-2 Effect of Rubble Modulus of Elasticity on the Drip Shield Deformed Shape at the Onset of Structural Instability, (a) E_r = 0 MPa and (b) E_r = 100 MPa 4-4
4-3 Vertical Loading Carrying Capacity Versus Horizontal Displacement at Critical Column Section for Different Rubble Modulus of Elasticity 4-5
4-4 Dependence of Vertical Load Carrying Capacity on Rubble Modulus of Elasticity . . . 4-5
4-5 Effect of Lateral Loading Asymmetry on the Drip Shield Deformed Shape at the Onset of Structural Instability (a) Symmetry and (b) Lateral Loading Asymmetry of 150 Percent 4-7
4-6 Effect of Lateral Loading Asymmetry on the Drip Shield Bending Moment Diagram at the Onset of Structural Instability (a) Symmetry Loading and (b) Lateral Loading Asymmetry of 150 Percent 4-8
4-7 Vertical Load Carrying Capacity Versus Horizontal Displacement at Critical Column Section for Different Levels of Lateral Loading Asymmetry 4-8
4-8 Dependence of Vertical Load Carrying Capacity on Lateral Loading Asymmetry . . . 4-9
4-9 Dependence of Vertical Load Carrying Capacity on Percentage of Average Lateral Loading 4-10
4-10 Effect of Lateral Load on the Drip Shield Deformed Shape at the Onset of Structural Instability, Average Lateral Load to Vertical Load of (a) 0 and (b) 0.50 . . 4-11
4-11 Drip Shield Deformed Shape for a System with Simulated Differential Settlement of 100 mm [4 in] 4-13
4-12 Drip Shield Bending Moment Diagram for a System with Simulated Differential Settlement of 100 mm [4 in] 4-14
4-13 Dependence of Vertical Load Carrying Capacity on Invert Degradation 4-15
4-14 Vertical Load Carrying Capacity Versus Horizontal Displacement at Critical Column Section for Different Drip Shield Temperatures 4-16
4-15 Vertical Load Carrying Capacity Versus Horizontal Displacement at Critical Column Section for Drip Shield with Different Plate Thickness 4-16
4-16 Drip Shield Lateral Loading Pressure at Stage 1 4-18
4-17 Drip Shield Deformed Shape at Stage 1 4-19
4-18 Drip Shield Deformed Shape at Stage 2 4-19
4-19 Effect of Stage Loading on Vertical Load Carrying Capacity 4-20

5-1 Time Histories for the Three Orthogonal Directions Scaled at Mean Annual Frequency of Exceedance of 10^{-6} for Loma Prieta Ground Earthquake, 1989 (Record 13, Gilroy Arr #6) (a) Velocities and (b) Accelerations 5-6
5-2 Envelope Response Spectra (5 Percent-Damped) at Emplacement Level for Mean Annual Frequency of Exceedance of 10^{-6} 5-7

FIGURES (continued)

Section Page

5-3 Individual Peak Ground Velocity and Peak Ground Acceleration for the Subset of 15 Ground Motions, Mean Annual Frequency of Exceedance of 10^{-5} (a) Peak Ground Velocity and (b) Peak Ground Acceleration 5-8
5-4 Individual and Statistical Peak Ground Velocity and Peak Ground Acceleration Data for the Subset of 15 Ground Motions, Mean Annual Frequency of Exceedance of 10^{-5} (a) Peak Ground Velocity and (b) Peak Ground Acceleration . . 5-9
5-5 Envelope Response Spectra (5 Percent-Damped) at Emplacement Level for Mean Annual Frequency of Exceedance of 10^{-6} 5-10
5-6 Envelope Response Spectra (5 Percent-Damped) at Emplacement Level for Mean Annual Frequency of Exceedance of 10^{-7} 5-10
5-7 Individual and Statistical Peak Ground Velocity and Peak Ground Acceleration Data for the Subset of 15 Ground Motions, Mean Annual Frequency of Exceedance of 10^{-6} (a) Peak Ground Velocity and (b) Peak Ground Acceleration . 5-11
5-8 Individual and Statistical Peak Ground Velocity and Peak Ground Acceleration Data for the Subset of 15 Ground Motions, Mean Annual Frequency of Exceedance of 10^{-7} (a) Peak Ground Velocity and (b) Peak Ground Acceleration . 5-12
5-9 Deformed Shape Under Baseline Loading Configuration (Scaled to a Target P_v = 180 KPa [26 psi]) 5-15
5-10 Horizontal and Vertical Accelerations at the Crown Apex. 5-16
5-11 Drip Shield Deformed Shape at the Onset of Structural Instability. 5-16
5-12 Horizontal and Vertical Accelerations at the Crown Apex. 5-17
5-13 Drip Shield Deformed Shape at the Onset of Structural Instability. 5-17
5-14 Accelerations Time Histories for the Three Orthogonal Directions Scaled at Mean Annual Frequency of Exceedance of 10^{-5} for Whitter Narrows Earthquake, 1987 (Record 10, Station San Gabriel) 5-18
5-15 Horizontal and Vertical Accelerations at the Crown Apex. 5-18
5-16 Drip Shield Deformed Shape at the Onset of Structural Instability. 5-19
5-17 Drip Shield Deformed Shape at the Onset of Structural Instability. 5-20

TABLES

Table Page

2-1 Drip Shield Material Property Data of 150 °C [302 °F] 2-10
2-2 Drip Shield Material Data for Modeling Post-Yield Behavior at 150 °C [302 °F] 2-10
2-3 Elastic Parameters of Various Soils 2-11
2-4 Elastic Parameters of Various Soils 2-12
2-5 System Parameter Values for Computing Soil Spring Constants 2-14

3-1 Bending Strength Capacity of Average Cross Sections Used in the Drip Shield Frame Model 3-2
3-2 Comparison of Displacements from ABAQUS Finite Element Model and SAP2000 Drip Shield Frame Model 3-14
3-3 Joint Reactions, Cases I and II 3-14
3-4 Selected Drip Shield Node Displacements for “Normalized” Baseline Loading Pattern 3-17
3-5 Drip Shield Reactions for “Normalized” Baseline Loading Pattern 3-18

4-1 Cases for Sensitivity Study of Lateral Loading Asymmetry 4-6
4-2 Cases for Sensitivity Study of Percentage of Average Lateral Loading 4-9
4-3 Drip Shield Reactions and Friction Force for Several Percentage of Average Lateral Loading Cases 4-10

5-1 Site Peak Ground Velocity for the Waste Emplacement Level 5-4
5-2 Ground Motion Proposed for Seismic Postclosure Analyses 5-5
5-3 Multiple Seismic Events During the Regulatory Period Based on a Poisson Distribution for Several Mean Annual Frequency Exceedance 5-14

ACKNOWLEDGMENTS

This report was prepared to document work performed by the Center for Nuclear Waste Regulatory Analyses (CNWRA) for the U.S. Nuclear Regulatory Commission (NRC) under Contract No. NRC–02–02–012. The activities reported here were performed on behalf of the NRC Office of Nuclear Material Safety and Safeguards, Division of High-Level Waste Repository Safety. This report is an independent product of CNWRA and does not necessarily reflect the views or regulatory position of NRC.

The authors thank B. Dasgupta and F. Ferrante for their technical reviews and W. Patrick for programmatic review of this report. The authors also express their appreciation to the NRC staff M. Nataraja and Y. Kim for their advice and counsel during planning and conducting the numerical analyses. The authors also appreciate A. Ramos for providing word processing support in the preparation of the document and E. Hanson for editorial review.

QUALITY OF DATA, ANALYSES, AND CODE DEVELOPMENT

DATA: All CNWRA-generated original data contained in this report meet quality assurance requirements described in the Quality Assurance Manual (Geosciences and Engineering Division, 2005). Sources of other data should be consulted for determining the level of quality of those data. The work presented in this report is documented in Scientific Notebooks 391, 409, 417, and 656.

ANALYSES AND CODES: Finite element and structural analyses in this report were conducted by CNWRA using the commercial computer codes ABAQUS/Standard Version 6.4 (ABAQUS, Inc., 2004) and SAP2000 Version 8.3.1 (Computer and Structures, Inc., 2004). ABAQUS/Standard Version 6.4 (ABAQUS, Inc., 2004) and SAP2000 Version 8.3.1 (Computer and Structures, Inc., 2004) are controlled under the software quality assurance procedure Technical Operating Procedure-018, Development and Control of Scientific and Engineering Software). Spreadsheet calculations were accomplished using Microsoft Excel® (Microsoft Corporation, 2002).

REFERENCES

ABAQUS, Inc. “ABAQUS User’s Manual.” Version 6.4. Providence, Rhode Island: ABAQUS, Inc. 2004.

Computers and Structures, Inc. “SAP2000 Version 8.3.1, Integrated Software for Structural Analysis and Design.” Berkeley, California. Computers and Structures, Inc. 2004.

Geosciences and Engineering Division. “Quality Assurance Manual” San Antonio, Texas: Geosciences and Engineering Division. 2005.

Microsoft Corporation. “Microsoft Excel 2002.5P3.” Redmond, Washington: Microsoft Corporation. 2002.

1 INTRODUCTION

1.1 Background

During the last two decades, the U.S. Department of Energy (DOE) has studied the Yucca Mountain site in Nevada to determine whether it is suitable for building a geologic repository for the disposal of the nation's spent nuclear fuel and high-level radioactive waste (DOE, 1998a). If the repository is approved, these radioactive materials will be encapsulated in waste packages and emplaced in tunnels excavated about 350 m [1,148 ft] below the surface and 225 m [738 ft] above the water table. Subsequently, drip shields will be placed over the waste packages. DOE is required by regulation to include at least one engineered barrier. The current proposed design includes as engineered barriers the emplacement drift, drip shield, waste package, multipurpose canister, spent fuel cladding, waste package pallet, and drift invert system. The engineered barriers are intended to work with the natural barriers—the geology and climate of Yucca Mountain—to contain and isolate nuclear waste for thousands of years. The barrier components, therefore, include materials compatible with the underground thermal and geochemical environment of the tunnels (DOE, 1998).

A U.S. Nuclear Regulatory Commission (NRC) and DOE technical exchange and management meeting on container life and source term of the potential repository at Yucca Mountain was held in Las Vegas, Nevada on September 12–13, 2000, The analysis of drip shield under repository environment and loading conditions was discussed at this technical exchange. An agreement on drip shield analysis, CLST.2.08 (Schlueter, 2000), was made between NRC and DOE after this meeting. This agreement asked for DOE to conduct drip shield analysis under static and seismic conditions taking into account the load of fallen rock on the drip shield.

The DOE response to NRC and DOE prelicensing agreement CLST.2.08 (Bechtel SAIC Company, LLC, 2003, Appendix K) included a summary of the results obtained from structural analyses of the drip shield subjected to accumulated rockfall rubble and dynamic rock block impact loads. In reviewing of these agreements (CNWRA, 2004), NRC indicated that DOE should address additional scenarios in the drip shield analysis to ensure a complete and high-quality license application. Specifically, NRC stated that the drip shield should be analyzed considering static loading due to accumulated rockfall rubble, and that the rubble should be considered when assessing the response of the drip shield to seismic ground motions. NRC also requested drip shield analyses for higher temperatures, for low-temperature creep, invert degradation, etc. These additional analyses will provide basis for evaluating whether the performance objectives for the repository after permanent closure are achieved (10 CFR §63.113).

This study independently evaluates the structural performance of the drip shield, an engineered barrier that limits the amount of water contacting the waste package as a result of seepage into the near-field environment. Although the original drip shield function was limited to protecting the waste package from dripping water, DOE is currently attempting to design the drip shield to protect the waste package from drift degradation. Therefore, the drip shield would have to be able to withstand rockfall impacts and static and dynamic (seismic) loading pressures originated by the accumulated rockfall rubble. The drip shield structural performance is relevant not only because it delays waste package corrosion, but also because a drip shield structural failure would cause drip shield-waste package interaction. As a result of this interaction, the waste package could experience high localized plastic stresses in the immediate regions where the drip shield bulkheads and longitudinal stiffeners, transfer the loads to the waste package.

The structural performance evaluation of this report refers to the current DOE drip shield design (Bechtel SAIC Company, LLC, 2004a). This updated design incorporates additional reinforcement of the drip shield crown in both transverse and longitudinal directions and is approximately one foot higher than the former design. This report investigates the static and dynamic drip shield structural performance under the presence of accumulated rockfall rubble. The system behavior largely depends on the distribution of load on the drip shield surface, and on the assumed system parameters. Because of large uncertainties in these variables, models with different system parameters and loading configurations are evaluated.

1.2 Objective and Scope

The objective of this study is to independently evaluate the structural response of the drip shield when subjected to static and dynamic loading under the presence of accumulated rockfall rubble. The analyses are used to compute the onset of drip shield structural instability as a function of the vertical load carrying capacity. The potential failure modes under mechanical loads and the main parameters affecting the drip shield strength capacity are identified.

The report focuses on the drip shield structural performance under different static loading configurations, as well as its performance under seismic excitations. A number of parameters that may modify the vertical load carrying capacity of the structure are investigated. The relationship between the drip shield strength capacity and the variation of these parameters will form the basis for the updated MECHFAIL abstractions used in Total-system Performance Assessment computer code (Mohanty, et al., 2002). These abstractions will be presented in a subsequent report.

This study does not address drip shield performance under rock block impact because Gute, et al. (2003) concluded that this is not a critical loading scenario. In addition, the expected structural damage due to rock block impact is smaller for the updated drip shield because its roof has been reinforced. Other phenomena contributing to drip shield structural degradation that are not included in this study are stress corrosion cracking, localized corrosion, fabrication flaws, weld residual stresses, hydrogen embrittlement, and creep.

This report is organized into six chapters. The introduction and scope are discussed in Chapter 1. Chapter 2 describes the main characteristics of the drip shield structure (e.g., geometry, material, and boundary conditions). An ABAQUS (ABAQUS, Inc., 2004) drip shield finite element model is introduced in this chapter. The structural response of the ABAQUS finite element model for selected loading configurations is presented, as well as calculations of moment-rotation relationships and drip shield-rubble interaction.

Chapter 3 describes the SAP2000 (Computer and Structures, Inc., 2004) drip shield frame model. This model is used for the sensitivity study for static loading conditions and seismic analyses. The accuracy of the SAP2000 model results, as compared to the ABAQUS finite element model, is discussed. Also, the methodology used to obtain the structural capacity of the drip shield at the onset of structural instability is described in terms of the baseline drip shield model.

The sensitivity study is discussed in Chapter 4, where the effects of several system parameters and loading conditions on the drip shield structural response are investigated. Among the evaluated parameters are the static loading configurations, temperature of the drip shield-rubble

modulus of elasticity, generalized corrosion of the drip shield plates, degradation of the invert, and stage loading.

The seismic loads on the drip shield response are evaluated in Chapter 5 by means of nonlinear dynamic time history analyses. The chapter discusses the main assumptions and the selection of the acceleration time histories used in the seismic analyses.

Conclusions regarding the drip shield structural performance are presented in Chapter 6. Finally, there are three appendices. Appendix A presents the calibration performed in order to obtain the stiffness properties of the drip shield frame model. Appendix B is a summary of the main results reported by DOE (Bechtel SAIC Company, LLC, 2004a) regarding the expected drip shield pressures due to static and dynamic loading conditions. Appendix C computes the bearing capacity of the invert.

2 DRIP SHIELD FINITE ELEMENT MODEL

2.1 Introduction

The drip shield is part of several engineered barrier subsystems that the U.S. Department of Energy (DOE) is proposing to use at the potential geologic repository at Yucca Mountain, Nevada. Figure 2-1 presents a typical cross section of the Yucca Mountain tunnels (CRWMS M&O, 2001). The drip shields will be installed at the end of the preclosure period, and their function will be to protect the waste packages from water intrusion and rockfall loading. The drip shield sections will be uniformly sized such that one design will be used over all waste package types. The sections will be interlocked to prevent separation between them. The only initial drip shield restraint is the friction developed between the drip shield base and the invert surface because the drip shield is a free-standing structure with no physical attachments to the drift invert.

The drip shield analyzed in this report corresponds to an updated design proposed by DOE (Bechtel SAIC Company LLC, 2004a) (Figure 2-2a). Each drip shield section has a length of 5,805 mm [228.5 in], a cross section width of 2,533 mm [99.7 in], and a total height of 2,886 mm [113.6 in]. The drip shield consists of Titanium Grade 7 plates that are supported with frames made of Titanium Grade 24 equally spaced at each 1,070 mm [42.1 in]. The drip shield base is made of Nickel Alloy N6022, commonly referred to as Alloy 22; and is the only drip shield structural component not made of titanium. According to DOE nomenclature (Bechtel SAIC Company, LLC, 2004a), the bulkhead refers to the reinforcing curve beam located at the drip shield crown, and the support beams are actually the columns of the drip shield frames spaced at 1,070 mm [42.1 in] (Figure 2-2a). The updated drip shield model reinforces the bulkhead with a bottom flange of 136 mm [5.35 in] (see Figures 2-2 and 2-3). The new model also incorporates three longitudinal stiffeners on the drip shield crown (Figure 2-2b), and is approximately one foot higher than the former design. There are additional drip shield modifications (e.g., the shape and location of the lifting assembly) but they do not affect drip shield performance.

If the drift degrades, the drip shield may be subjected to dynamic impact from falling rock blocks and from static and dynamic loads due to the accumulated rockfall rubble (Gute, et al., 2003). Based on its drift degradation analysis (Bechtel SAIC Company, LLC, 2004b), DOE concluded that (i) only a small fraction of the emplacement drifts (i.e., those located in the lowest quality areas of the lithophysal rocks) will experience significant degradation from the combined effects of thermal loading and potential time-dependent weakening of rock, and (ii) seismic ground motions from a potential earthquake with an annual frequency of 10^{-5} or less per year would cause widespread drift degradation. The DOE conclusion implies that the occurrence of accumulated rockfall rubble would depend on the probability of occurrence of such earthquakes. Staff analysis, however, indicates that drift degradation induced by repository thermal loading or time-dependent rock weakening (with or without seismic loading) could be more widespread than that estimated by DOE (Ofoegbu, et al., 2004). To address the uncertainties regarding the occurrence of rockfall rubble, DOE indicates the drip shield would be designed to withstand loading from a completely collapsed drift (Bechtel SAIC Company, LLC, 2004c).

The evaluation of the drip shield structural performance under the presence of rockfall rubble is the main objective of this study. This evaluation includes three ABAQUS (ABAQUS, Inc.,

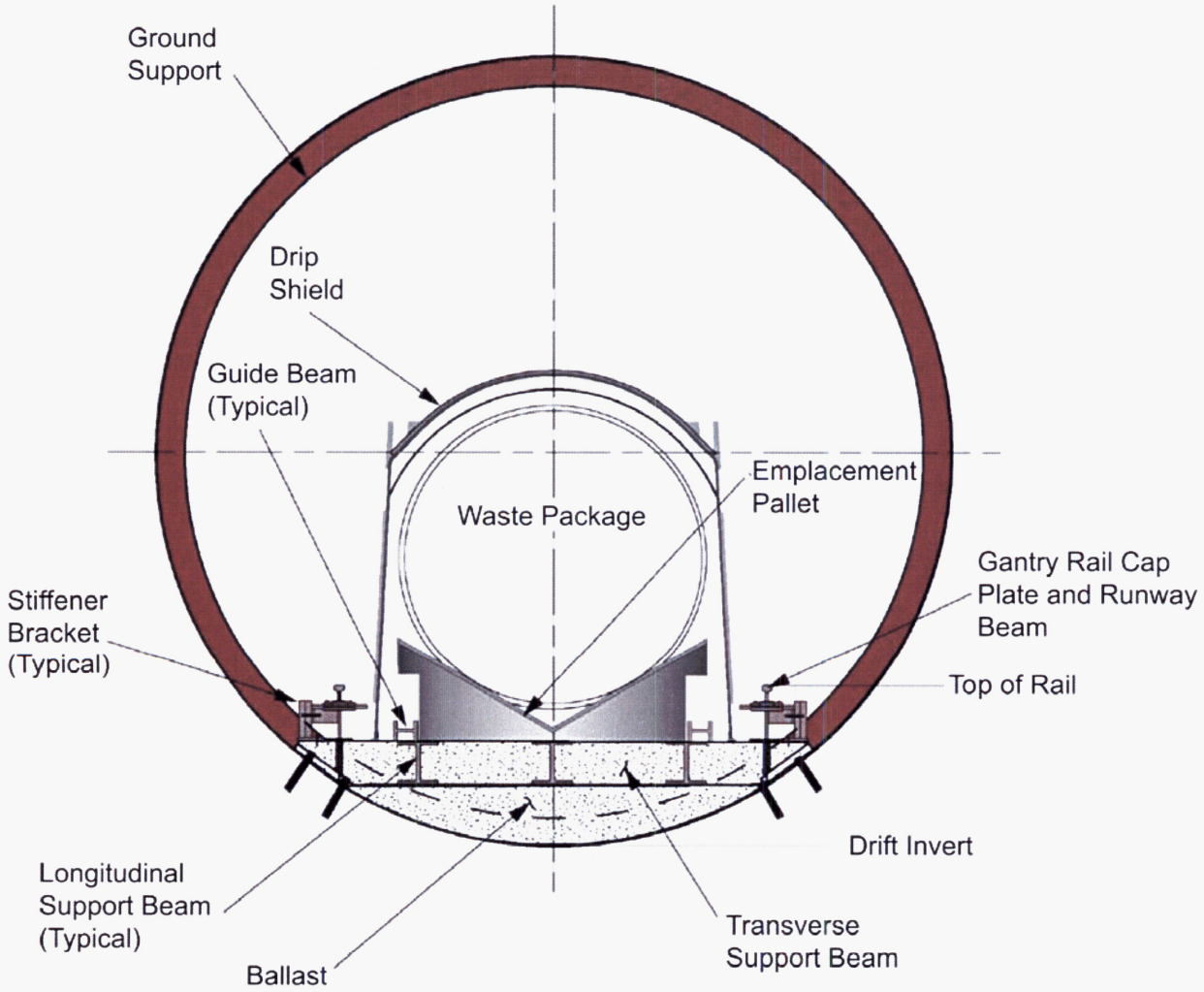

2004) finite element models and a drip shield frame model created in the structural program SAP2000 (Computers and Structures, Inc., 2004). The drip shield finite element model presented in this chapter has three goals: (i) to validate the SAP2000 frame model used for the sensitivity study, (ii) to provide the frame model developed in SAP2000 with rock rubble equivalent spring constants, and (iii) to develop a moment-rotation relationships for the drip shield side-roof transition, and for support beams (columns) to be used in the drip shield frame model (see Section 3.1.2). To reach these objectives, three distinct ABAQUS finite element models were developed. The first model is a detailed finite element model of the drip shield structure (Section 2.2) used for validating the frame model. The moment-rotation relationships for the drip shield columns are obtained using a modified detailed finite element model with different boundary conditions. The second is a specialized model of the drift wall, rock rubble,

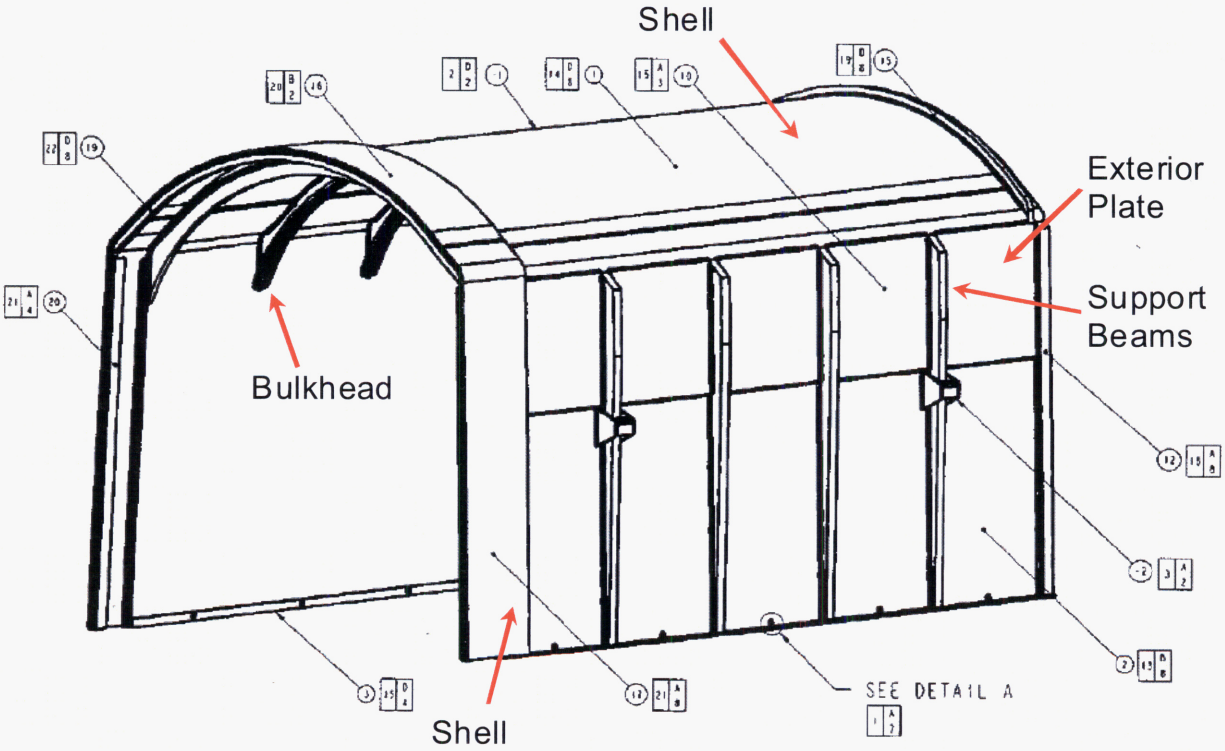

Figure 2-2a. Isometric of Updated Drip Shield (Bechtel SAIC Company, LLC, 2004a)

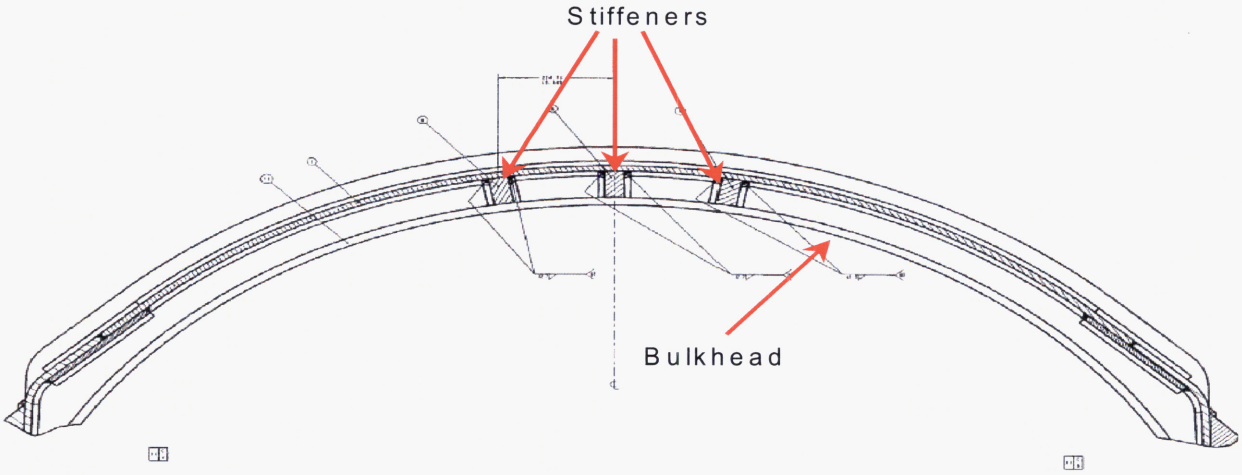

Figure 2-2b. Drip Shield Crown Section (Bechtel SAIC Company, LLC, 2004a)

and drip shield side wall (Section 2.3.1) that is used for obtaining the spring constants. The third is a model of bulkhead corner section, which is used to obtain a moment-rotation curve for this region (Section 2.3.2.1).

2.2 Description of Detailed ABAQUS Drip Shield Finite Element Model

The detailed drip shield finite element model was utilized to verify the accuracy of the drip shield frame model introduced in Chapter 3. This model was also used to obtain moment-rotation relationships at several locations of the drip shield column, which were used in the drip shield frame model. The finite element model consisted of the following main components: (i) the Titanium Grade 7 shell plate, (ii) interior and exterior plates, (iii) the Titanium Grade 24 bulkhead, support beams, and (iv) longitudinal stiffeners; and the Alloy 22 base plate (Figure 2-3). This finite element model no longer included rockfall rubble, the drift wall, or invert surfaces (Gute, et al., 2003). These modifications were made to improve the computational efficiency of the model. That is, a full contact analysis was previously required to model the rockfall rubble drip shield wall interaction which increased the computational time. Then uniform, normal, pressure loads were directly applied to the drip shield (Figure 2-4) to substitute for the pressure developed due to the presence of the rubble.

The structural and loading variations in the longitudinal direction were neglected. Thus, it was assumed that the drip shield segments, defined by the uniform spacing of the support beam and bulkhead reinforcing elements, repeat continuously in the axial direction. This assumption, as well as an imposed symmetric structural response, requires that only a quarter of this repeated drip shield frame section be modeled (Figure 2-3). This simplification allowed an adequate mesh density in the model without significantly increasing the computational time.

The original drip shield finite element model was constructed using a mixture of plate and solid elements (Gute, et al., 2003). Plate elements (three-dimensional quadrilaterals) were used for Titanium Grade 7 panel sections, and the drip shield base made of Alloy 22. Solid elements (hexahedrons) were used to represent the Titanium Grade 24 structural support beams and bulkhead components. The plate elements, however, were replaced by solid elements in the drip shield model of this study. This allows some drip shield regions with complicated geometry to be modeled with sufficient detail to accurately capture the associated complex nonlinearities that arise. An example of one of these regions is the drip shield corner, where the bulkhead transfers the load to the support beams. The support beams are Titanium Grade 24 external components that are welded to the Titanium Grade 7 plate, whereas the bulkhead is an internal Titanium Grade 24 member welded to the Titanium Grade 7 plate. Therefore, the frame transition from the support beam to bulkhead at the drip shield corner includes an intermediate Titanium Grade 7 panel that has to transfer the stresses between the Titanium Grade 24 components, which have a much larger yield strength (Figure 2-5).

In the drip shield design, the edges of the external and internal plates (Figures 2-2 and 2-3) are welded to the shell. In the drip shield finite element model, however, all the solid elements representing the external and internal plates were coupled to the solid elements of the shell. This approximation implies that full composite action takes place between these plates, and neglects the potential for high concentrated stresses at the zones where the external and internal plates are welded.

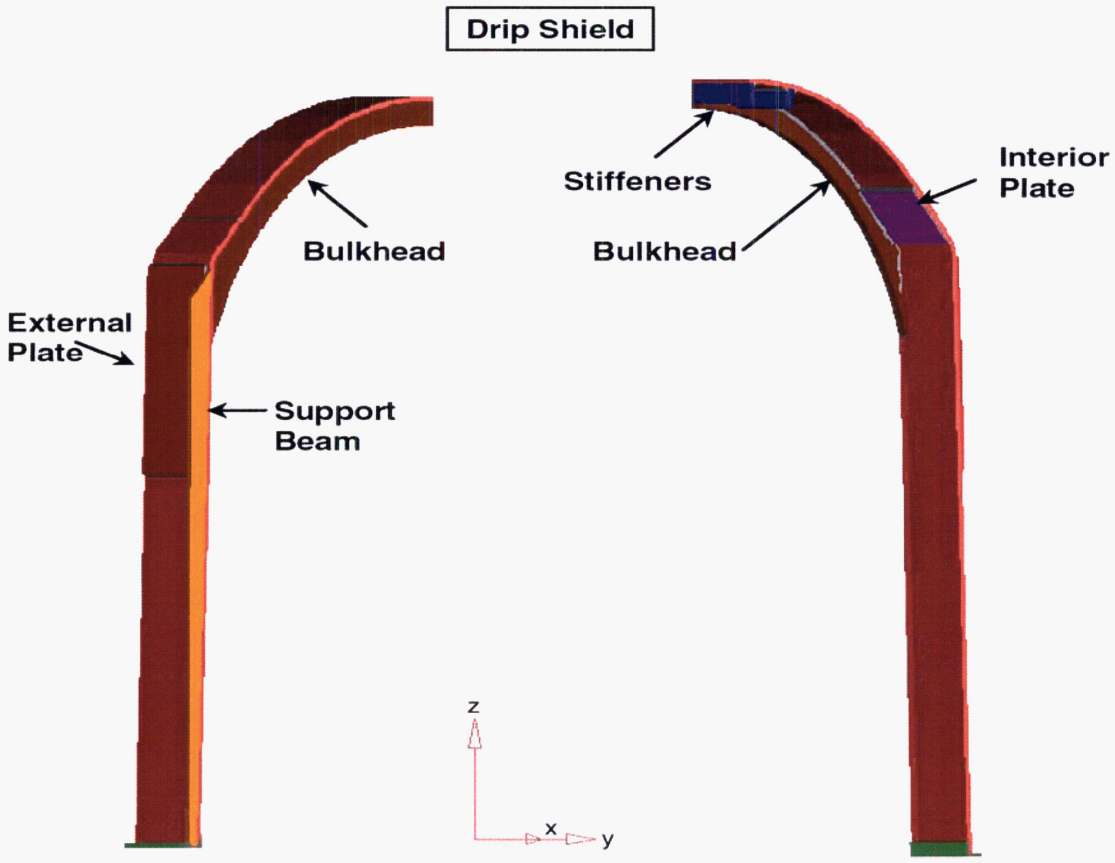

Figure 2-3. Isometric of Drip Shield Finite Element Model

The drip shield finite element model utilized elastic-plastic material behavior and large strain/rotation element formulations. The ABAQUS standard classical metal plasticity constitutive model was used to represent the bilinear behavior of Titanium Grade 7 and Titanium Grade 24. Specifically, the material was represented by a Von Mises yield surface with isotropic hardening. This classical metal plasticity constitutive model also employs an associated plastic flow rule (i.e., as the material yields, the inelastic deformation rate is in the direction normal to the yield surface). An additional common constraint in the context of classical metal plasticity is that the material maintains a constant volume while undergoing plastic deformation (i.e., plastic incompressibility).

2.2.1 Material of Drip Shield Finite Element Model

2.2.1.1 Drip Shield Material Properties

The materials proposed for the drip shield are Titanium Grade 7, Titanium Grade 24, and Nickel Alloy N6022, usually referred to as Alloy 22. The drip shield base will be made from Alloy 22, and the bulkhead and support beam will be made from Titanium Grade 24. All other drip shield components will be fabricated using Titanium Grade 7. The relevant material properties for the

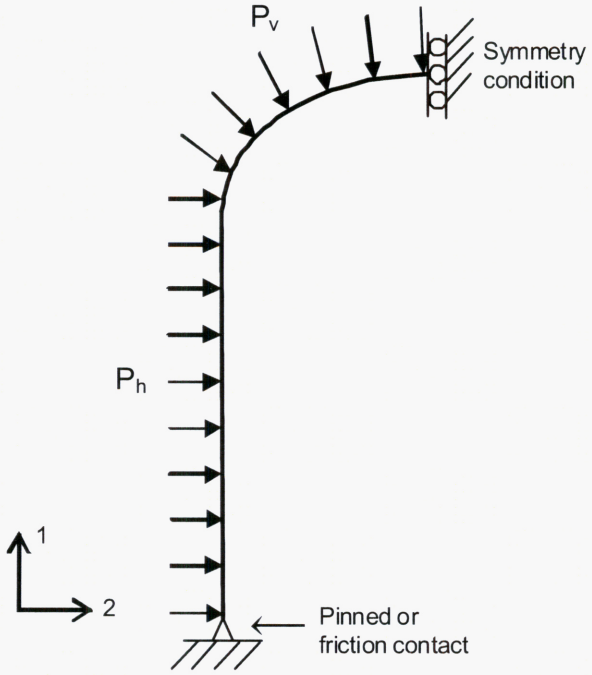

Figure 2-4. Drip Shield Finite Element Model with Uniform Normal Pressure

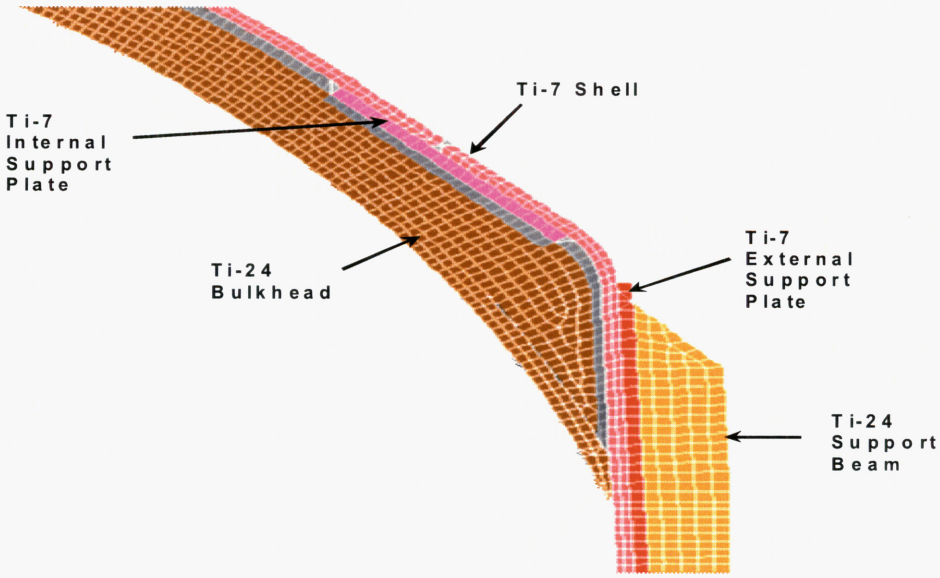

Figure 2-5. Drip Shield Corner Section

drip shield analyses are the yield stress (f_y), ultimate tensile stress (f_u), modulus of elasticity (E), and the nominal elongation (ε_{nom}). These properties are used to approximate a bilinear stress-strain curve to model the inelastic behavior. A large part of the data has been obtained from the ASME International (2001).

The material properties largely depend on the temperature, a parameter that may dramatically change during the regulatory period. For computing the drip shield structural response, DOE has used material properties associated with a temperature of 150 °C [302 °F] (Bechtel SAIC Company, LLC, 2004d). DOE has argued that properties at this temperature are adequate because the drip shield will not exceed this temperature in 98.5 percent of the compliance period. The modulus of elasticity for Titanium Grade 7 was obtained from Table TM–5 of the ASME International (2001). For Titanium Grade 24, however, temperature-dependent values for the yield stress, ultimate strength, and modulus of elasticity are not readily available. As a result, Titanium Grade 5 is used as a surrogate for Titanium Grade 24 because the compositions of these materials are similar [Titanium Grade 24 contains 0.04 to 0.08 percent palladium (Gute, et al., 2003)]. The Military Handbook: *Metallic Materials and Elements for Aerospace Vehicle Structures* (U.S. Department of Defense, 1998) and the Material Properties Handbook: *Titanium Alloys* (ASM International, 1994) both provide extensive material data for Titanium Grade 5.

Data from these references were used to develop the curves of Figure 2-6, which corroborate the dependence of yield stress and ultimate strength of titanium components on temperature. On the other hand, the modulus of elasticity exhibits a modest dependence on temperature (Figure 2-6c). Titanium Grade 5 (surrogate for Titanium Grade 24) not only exhibits a much higher yield and ultimate stress than Titanium Grade 7, but also exhibits less material degradation at high temperatures. The material properties for Alloy 22 are relatively unaffected by exposure to the expected emplacement drift temperature with respect to their room temperature values.

These material properties correspond to the engineering stresses and strains. Because the drip shield may experience large deformations and inelastic strains, however, the ABAQUS standard finite element program (when using the NLGEOM option) requires that the material property data, which may be in terms of engineering or nominal stress, be converted to true stress (Cauchy stress), and that the engineering or nominal strain be converted to logarithmic strain (ABAQUS, Inc., 2004). Conversions are made as follows:

$$\sigma_{true} = \sigma_{nom}\left(1 + \varepsilon_{nom}\right) \tag{2-1}$$

$$\varepsilon_{ln}^{pl} = ln\left(1 + \varepsilon_{nom}\right) - \frac{\sigma_{true}}{E} \tag{2-2}$$

where

σ_{true} = true stress (Cauchy stress)
σ_{nom} = nominal stress (engineering stress)
ε_{ln}^{pl} = logarithmic plastic strain

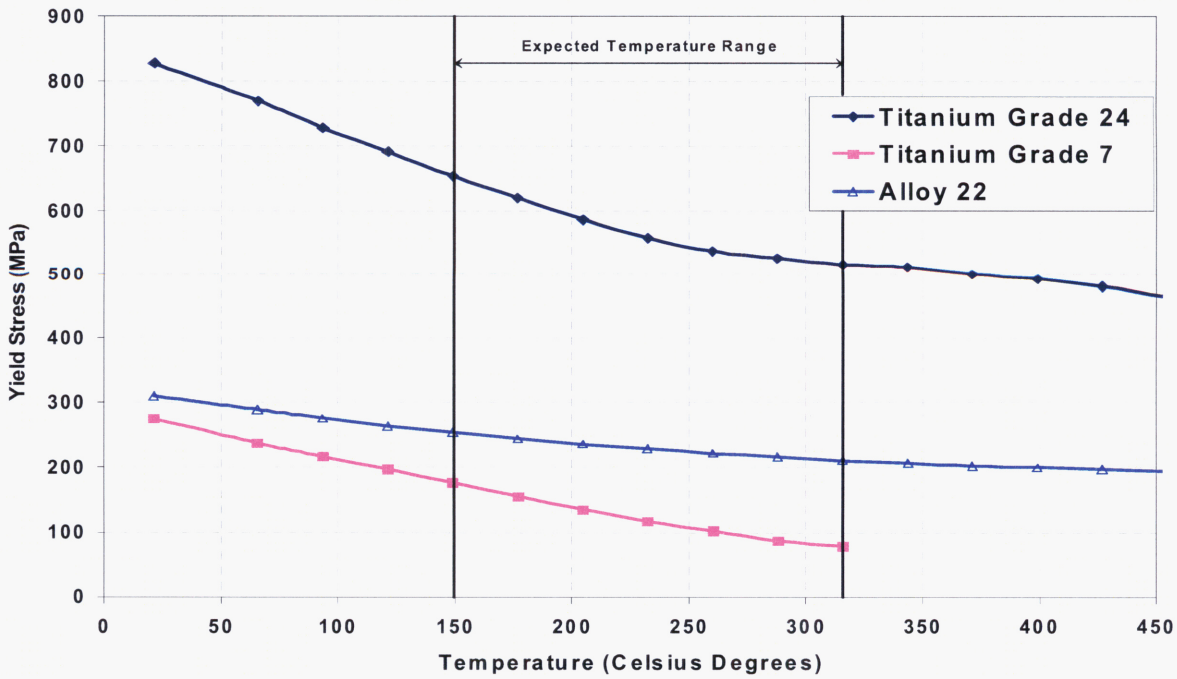

Figure 2-6a. Dependence of Yield Tensile Stress on Temperature

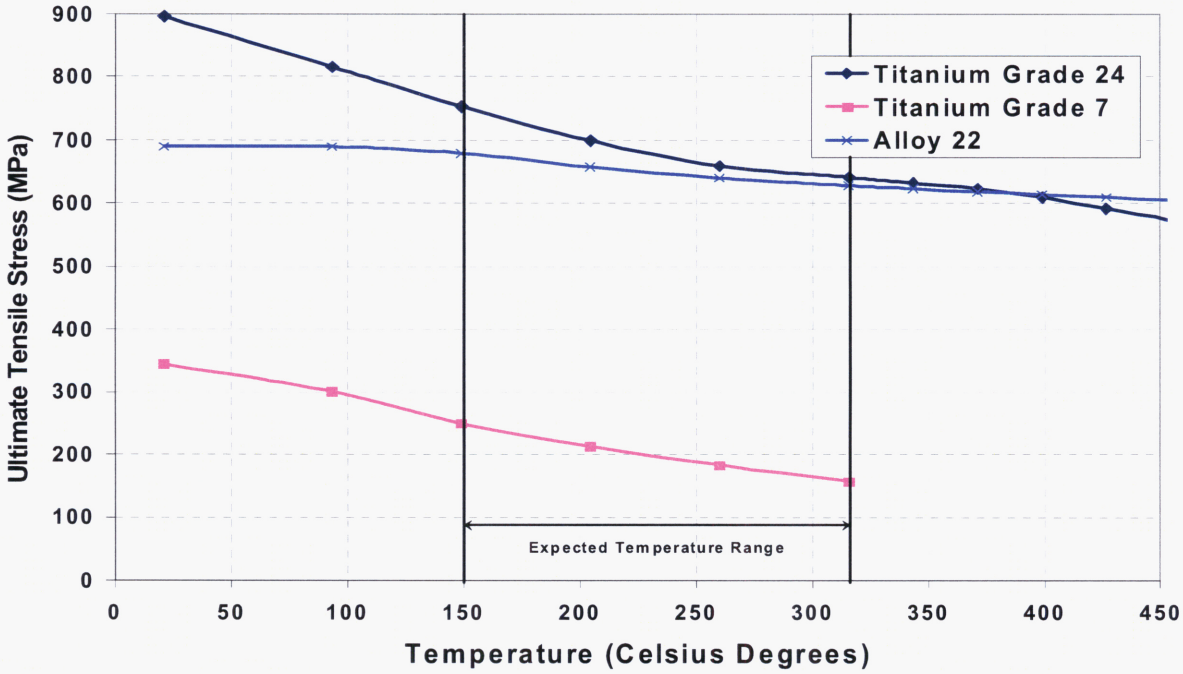

Figure 2-6b. Dependence of Ultimate Stress on Temperature

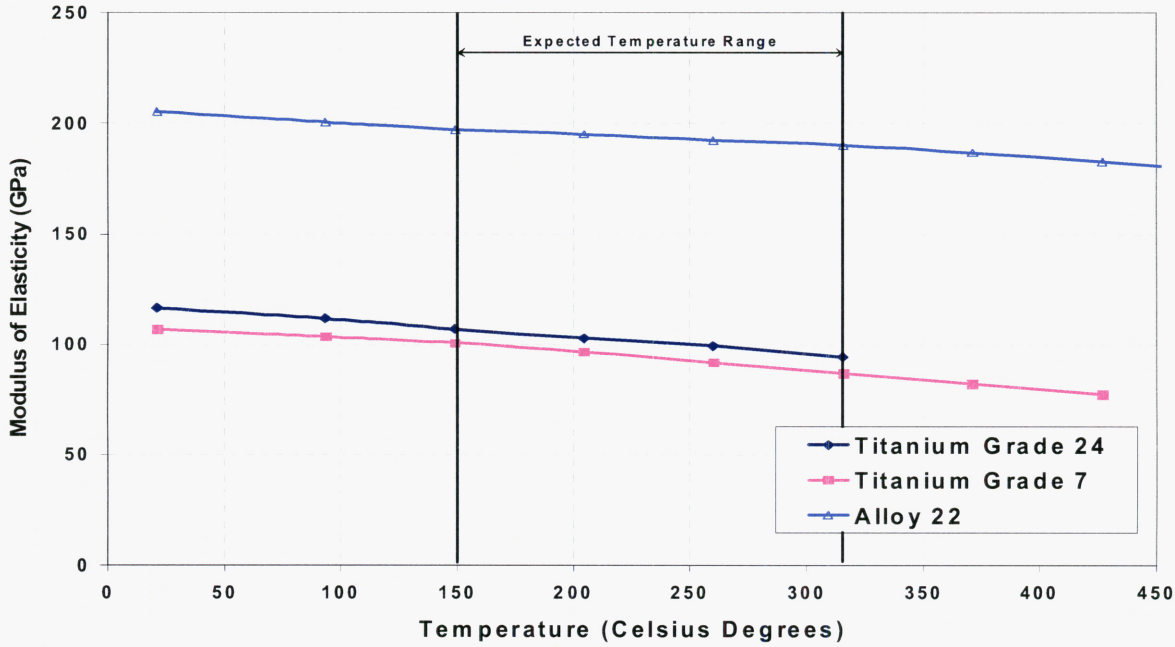

Figure 2-6c. Dependence of Modulus of Elasticity (*E*) on Temperature

ε_{nom} = nominal strain (engineering strain)
E = modulus of elasticity (Young's modulus)

Tables 2-1 and 2-2 summarize the material properties used for the drip shield analyses at 150 °C [302 °F], except for the Poisson's ratio values that correspond to room temperature. A bilinear approximation of the true stress-logarithmic strain curves for Titanium Grade 7 and Titanium Grade 24 assuming a drip shield temperature of 150 °C [302 °F] is presented in Figure 2-7. The modulus of elasticity for Titanium Grade 7 and Titanium Grade 24 is very similar. Thus, the two materials will undergo elastic deformation without creating large stress concentrations in the material interface. Figure 2-7 also indicates that Titanium Grade 7 can accommodate much larger ductile displacements than Titanium Grade 24. On the other hand, Titanium Grade 24 has more than three times the yield strength of Titanium Grade 7. Therefore, Titanium Grade 24 remains in the elastic range under large stresses, but is susceptible to potential brittle failure under nonlinear incursions.

2.2.1.2 Rockfall Rubble Material Properties

In this chapter, the rubble material properties were used only in the specialized finite element model (Section 2.3.1) to obtain the equivalent spring constants required in the drip shield frame model (Chapter 3). The rubble behind the drip shield sides may contribute to the structural resistance of the drip shield if side-sway and outward deformation of the drip shield support beams compress the rubble, thereby developing a passive resistance. The amount of passive resistance would vary with the confining pressure, the magnitude of compression, and any compaction from previous rubble compression (e.g., Lambe and Whitman, 1969). The passive resistance would be controlled by several characteristics of the rubble (e.g., particle size and shape distributions, degree of wetness, strength of individual particles or blocks, and porosity) (e.g., Marsal, 1973). Values of the elastic stiffness parameters, such as the modulus of

Table 2-1. Drip Shield Material Property Data at 150 °C [302 °F]			
Material Name	**Density, tonne/m^3 [lb/in^3]**	**Young's Modulus, GPa [psi]**	**Poisson's Ratio**
Titanium Grade 7	4.512 [0.163]*	100.7 [14.6 × 10^6]†	0.32‡
Titanium Grade 24	4.512 [0.163]*	107.2 [15.5 × 10^6]¶	0.32‡
Alloy 22	8.691 [0.314]‖	197.2 [28.6 × 10^6]§	0.32‖

*ASME International. "ASME International Boiler and Pressure Vessel Code." New York City, New York: ASME International. Table NF–2, Typical Physical Properties of Nonferrous Materials (Unalloyed Titanium). 2001.

†———. "ASME International Boiler and Pressure Vessel Code." Table TM–5, Moduli of Elasticity of Titanium and Zirconium for Given Temperatures. New York City, New York: ASME International. 2001.

‡———. "ASME International Boiler and Pressure Vessel Code." Table NF–1, Typical Mechanical Properties of Materials (Unalloyed Titanium). New York City, New York: ASME International. 2001.

§———. "ASME International Boiler and Pressure Vessel Code." Table TM–4, Moduli of Elasticity of High Nickel Alloys for Given Temperatures. New York City, New York: ASME International. 2001.

‖ASTM International. "Standard Specification for Low-Carbon Nickel-Molybdenum-Chromium, Low-Carbon Nickel-Chromium-Molybdenum, Low-Carbon Nickel-Chromium-Molybdenum-Copper, Low-Carbon Nickel-Chromium-Molybdenum-Tantalum, and Low-Carbon Nickel-Chromium-Molybdenum-Tungsten Alloy Plate, Sheet, and Strip." New York City, New York: ASTM International. 1998.

¶U.S. Department of Defense. "Military Handbook: Metallic Materials and Elements for Aerospace Vehicle Structures." Figure 5.4.1.1.4, Effect of Temperature on the Tensile and Compressive Moduli of Annealed Ti–6Al–4V Alloy Sheet and Bar. MIL–DBK–5H. Washington, DC: U.S. Department of Defense. 1998.

Table 2-2. Drip Shield Material Data for Modeling Post-Yield Behavior at 150 °C [302 °F]			
Material Name	**Yield Stress,* MPa [psi]**	**Ultimate Tensile Strength,* MPa [psi]**	**Log Normal Failure Strain, Percent**
Titanium Grade 7	174.1 [2.53 × 10^4]	299.5 [4.34 × 10^4]	17.93
Titanium Grade 24	658.1 [9.54 × 10^4]	827.0 [1.20 × 10^5]	8.76
Alloy 22	254.7 [3.69 × 10^4]	984.7 [1.43 × 10^5]	36.70

*Cauchy Stress

elasticity and Poisson's ratio, were selected based on literature information. For example, data from the laboratory testing of crushed aggregates and natural sand and gravel (Marsal, 1973) indicate that a significant variability of the elastic parameters should be expected.

The values of mechanical properties for rubble were estimated based on information available in the literature for cohesionless aggregates, such as natural sands and gravel or crushed rock. Rubble is expected to be similar to such aggregates because of being cohesionless (i.e., an assemblage of uncemented rock fragments), and having a wide range of particle sizes from a fraction of a millimeter to several centimeters, somewhat similar to a talus deposit. Tables 2-3

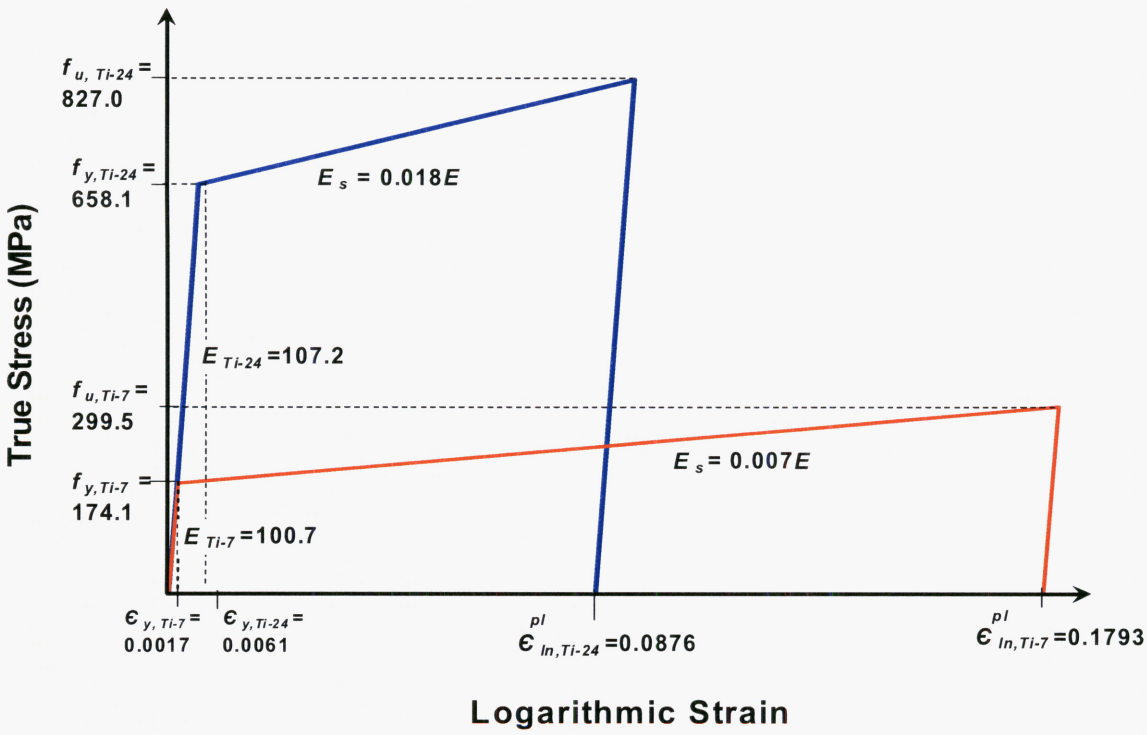

Figure 2-7. True Stress-Logarithmic Strain Curves for Titanium Grade 7 and Titanium Grade 24 at 150 °C [202°F]

Table 2-3. Elastic Parameters of Various Soils*

Type of Soil	Modulus of Elasticity, *E*		Poisson's Ratio, ν
	ksi (kips/in^2)	MPa (MN/m^2)	
Loose Sand	1.5–3.5	10.35–24.15	0.20–0.40
Medium Dense Sand	2.5–4.0	17.25–27.60	0.25–0.40
Dense Sand	5.0–8.0	34.50–55.20	0.30–0.45
Sand and Gravel	10.0–25.0	69.00–72.50	0.15–0.35

*Das, B.M. *Principles of Foundation Engineering*. 4th Edition. Pacific Grove, California. PWS-Kent Publishing. 1998.

and 2-4 present general values for the modulus of elasticity and Poisson's ratio for sands and gravel compiled by Bowles (1977) and Das (1998), respectively. Similar information is also available from Richart, et al. (1970) for round and angular-grained sand with a different void ratio and confining pressures. The value of the modulus of elasticity, *E*, for such materials is in the range of 30 to 150 MPa [4.35 to 21.75 Ksi] based on the information in Tables 2-3 and 2-4.

Table 2-4. Elastic Parameters of Various Soils*			
Type of Soil	**Modulus of elasticity, *E***		**Poisson's Ratio, ν**
	ksi (kips/in^2)	**MPa (MN/m^2)**	
Loose Sand	1.5–3.5	10.35–24.15	0.15
Dense Sand	7.0–12.0	48.30–82.80	0.20–0.40
Loose Sand and Gravel	7.0–20.0	48.30–138.00	—
Dense Sand and Gravel	14.0–28.0	96.60–193.20	—
*Bowles, H.E. *Foundation Analysis and Design*. 2nd Edition. New York City, New York: McGraw-Hill. 1977.			

Triaxial test data for crushed basalt tested under a confining pressure of 207 KPa [30 psi] (Marachi, et al., 1972) indicate a modulus of elasticity of approximately 50 MPa [7.2 Ksi] for such materials. However for the rockfall rubble that may surround the drip shield, it was estimated that the rubble modulus of elasticity may be as low as E_r = 10 MPa [4.35 Ksi] because of the lack of any significant compaction. For the drip shield baseline frame model introduced in Chapter 3, a modulus of elasticity value of 30 MPa [4.35 Ksi] was used based on the assumption that the stress-strain behavior of rockfall rubble is similar to the stress-strain behavior of crushed rock or natural sand and gravel. The sensitivity study of the drip shield strength capacity to variations of E_r was evaluated in Chapter 4.

2.2.2 Boundary Conditions

2.2.2.1 Kinematic Constraints

An axial symmetry condition was imposed on the drip shield that constrains translations and rotations out of the axial plane. This constraint is analogous to a two-dimensional plane strain assumption and implies that the static rockfall load is uniformly applied along the entire length of the drip shield. In order to enforce symmetry, the detailed drip shield finite element model precludes rotations and horizontal displacement of the drip shield crown apex. For most of the analyses, this model used a pinned restraint at the point where the Alloy 22 base contacts the invert. The pinned constraint is a valid approximation for the case in which the frictional force developed between the drip shield base and the invert surface overcomes the horizontal base reaction force. The assumption was validated using a finite element model that included a contact surface to account for the friction force developed between the drip shield base and the invert (see Section 2.3.3). The difference in response was negligible for both models (i.e., model with pinned constraint and model with contact surface), as long as the frictional force overcame the drip shield base horizontal reaction.

2.2.2.2 Loads

A uniform pressure was applied normal to the crown and side walls of the drip shield (Figure 2-4). Uniform pressure is considered a reasonable assumption for the drip shield crown according to the drip shield pressures obtained for a vertical ellipse degradation zone geometry (Gute, et al., 2003).

2.3 Drip Shield Finite Element Models and Results

The detailed drip shield finite element model was used to verify the accuracy of the drip shield frame model discussed in Chapter 3. Also, two input parameters for the frame model were obtained: the equivalent spring constants and the moment-rotation curves for critical sections.

2.3.1 Calculation of Spring Constants Using the Drip Shield Finite Element Model

A specialized drip shield finite element model was used to obtain the equivalent spring constants implemented in the drip shield frame model (Chapter 3). This model includes one drip shield side wall, the drift wall, and the rubble in between these two components (Figure 2-8). The drip shield side wall and the drift wall were modeled as rigid bodies, and the rubble was modeled as a solid continuum. First, the confining pressure was applied to the top surface of the rockfall rubble. Then, to obtain the rubble reaction force throughout the height of side wall, the wall was forced to compress the rubble pile using a prescribed displacement. The effect of confining pressure, rubble modulus of elasticity, and friction between the rock rubble and the drift wall on the effective rubble spring constant was evaluated. The Poisson's ratio was kept constant as $\nu = 0.17$, and the coefficient of friction between the rock rubble and the drip shield side wall was assumed as zero.

As indicated in Section 2.2.1.2, there is large uncertainty in the available rubble material property information. For instance, the modulus of elasticity increases as the confining pressure increases, and in general as the strain rate becomes higher. Because of this large variability, the equivalent spring constants were obtained for several drip shield finite element models with different combinations of rubble modulus of elasticity, E_r, overpressure, σ_o, and friction coefficient, μ, between the drift wall and the rubble. Table 2-5 summarizes the data used for the five evaluated cases.

The force-displacement relationships computed for each one of drip shield wall elements were grouped according to the location of the 12 equivalent springs of the frame drip shield model. The largest equivalent spring constant values at a drip shield height of 1,678 mm was mainly caused by the longer length of the top column section. Figure 2-9 presents the variation of spring constants with drip shield height for the five combinations of Table 2-5. Note that the force-displacement relationships are nonlinear because the compressed rubble tends to move upwards causing geometric nonlinearities. Thus, the spring constants are obtained as the average of each nonlinear relationship for the expected drip shield displacement interval. A comparison of Cases 2 and 4 indicates that the confining pressure is very relevant when there is no friction between the rubble and the drift wall (i.e., when the overpressure is the only factor preventing the rubble from moving upwards). Cases 3 and 5 have a friction coefficient of 0.4, however, and under this scenario the confining pressure is not relevant. Case 5 should render more realistic equivalent spring constants because accounts for friction between the drift wall and the rubble, and includes a vertical pressure that is between the reasonable lower and upper boundaries presented in Section 3.1.4.2. Therefore, the equivalent spring constants of Case 5 were used for most of the realizations of subsequent chapters.

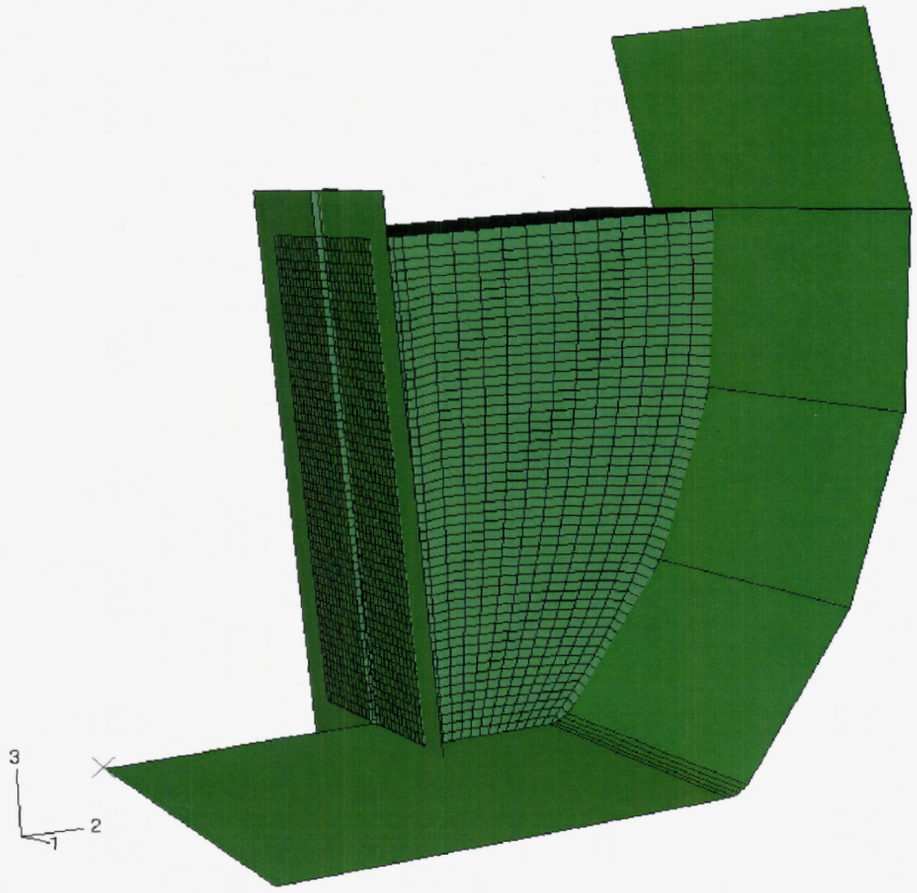

Figure 2-8. Drip Shield Finite Element Model for Obtaining Soil Spring Constants

Table 2-5. System Parameter Values for Computing Soil Spring Constants			
Case	**Over Pressure, σ_o (KPa)**	**Rubble Modus, E_r (MPa)**	**Friction Coefficient*, μ**
1	122	1	0.0
2	122	30	0.0
3	122	30	0.4
4	400	30	0.0
5	400	30	0.4
*This is the friction coefficient between the rock rubble and the drift wall.			

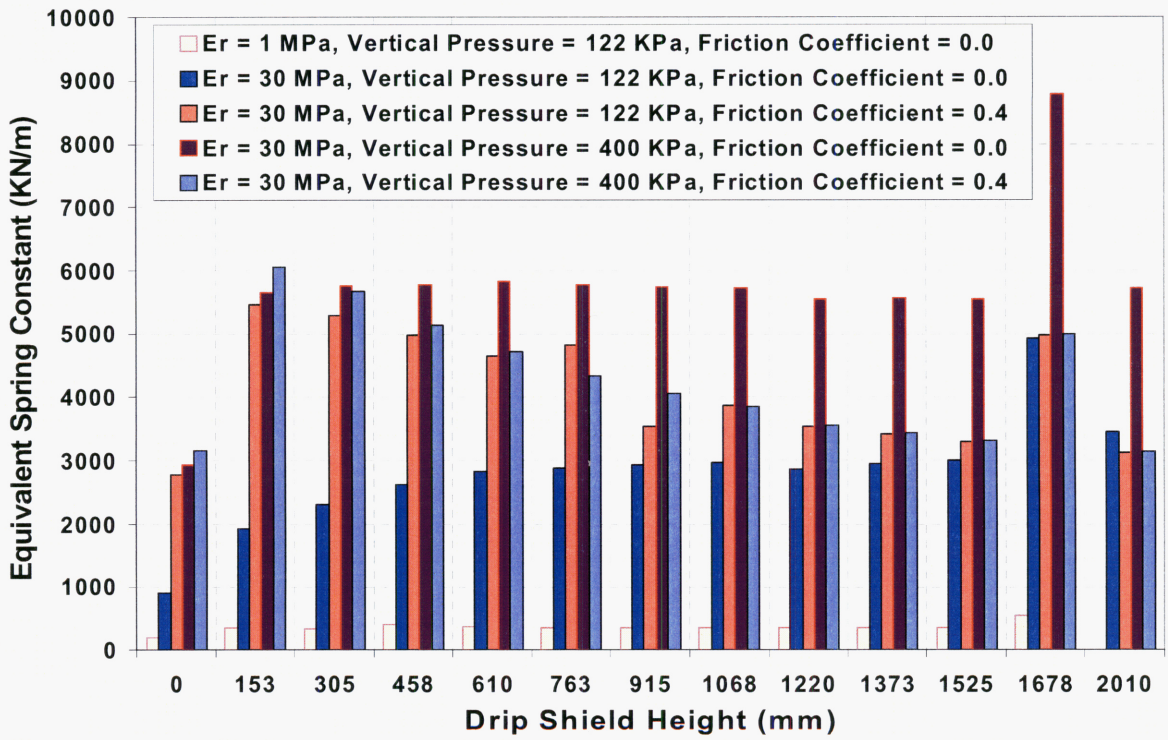

Figure 2-9. Variation of Soil Springs Constants With Drip Shield Height

2.3.2 Moment-Rotation Curves

The moment-rotation curves at several critical sections of the drip shield were developed using the ABAQUS (ABAQUS, Inc., 2004) model. This information is not conventionally obtained from finite element models; however, moment rotation curves are necessary to characterize the drip shield frame model presented in Chapter 3.

2.3.2.1 Drip Shield Corner

The frame transition from the Titanium Grade 24 support beams (columns) to the Titanium Grade 24 bulkhead (beams) requires transfer stress through a Titanium Grade 7 plate (see Figure 2-5). The modulus of elasticity for both titanium grades is very similar. The yield strength for Titanium Grade 24, however, is almost four times larger than that of Titanium Grade 7, which may imply that some sections of the sandwich component (i.e., Titanium Grade 7 plate) could completely yield early in the loading process, triggering a complex nonlinear interaction between the plates. The potential for early failure of the joint was investigated using a separate finite element model of the drip shield corner (Figure 2-10). This drip shield corner model was subjected to a moment load at the top of the bulkhead segment. The boundary conditions for this scaled-model are as follows: (i) the nodes defined in the plane at the base of the drip shield column, external support plate, and plate are constrained to remain within this plane; (ii) the base of the column is fixed; and (iii) the nodes that lie on the plane at the top of the bulkhead, external support plate, and shell the remains on the analytical rigid surface plane as it rotates.

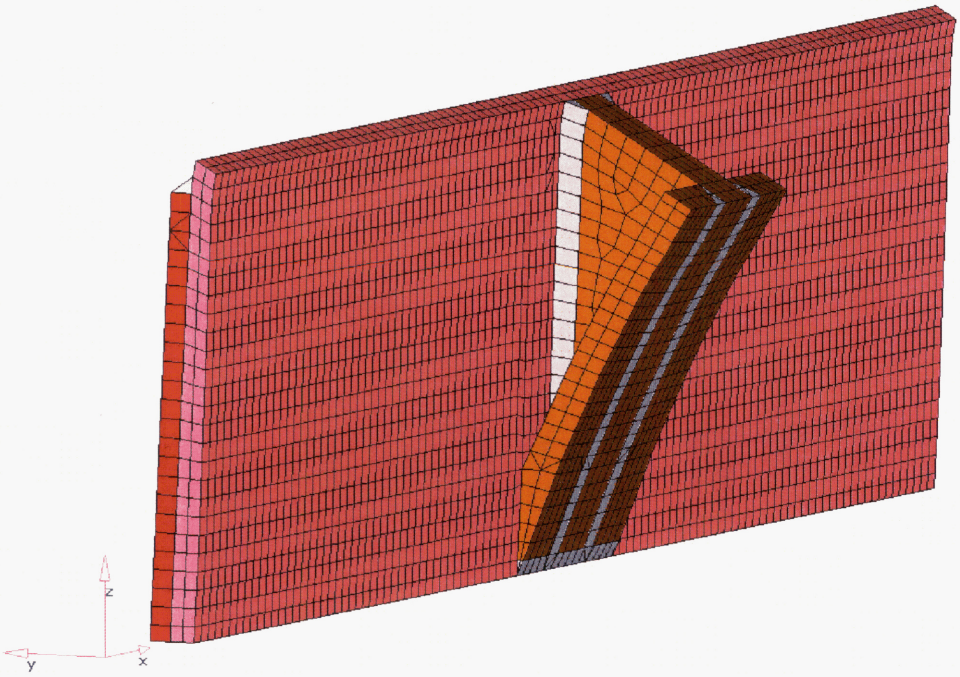

Figure 2-10a. Finite Element Model of the Drip Shield Corner to Obtain Moment-Rotation Curve (Interior View)

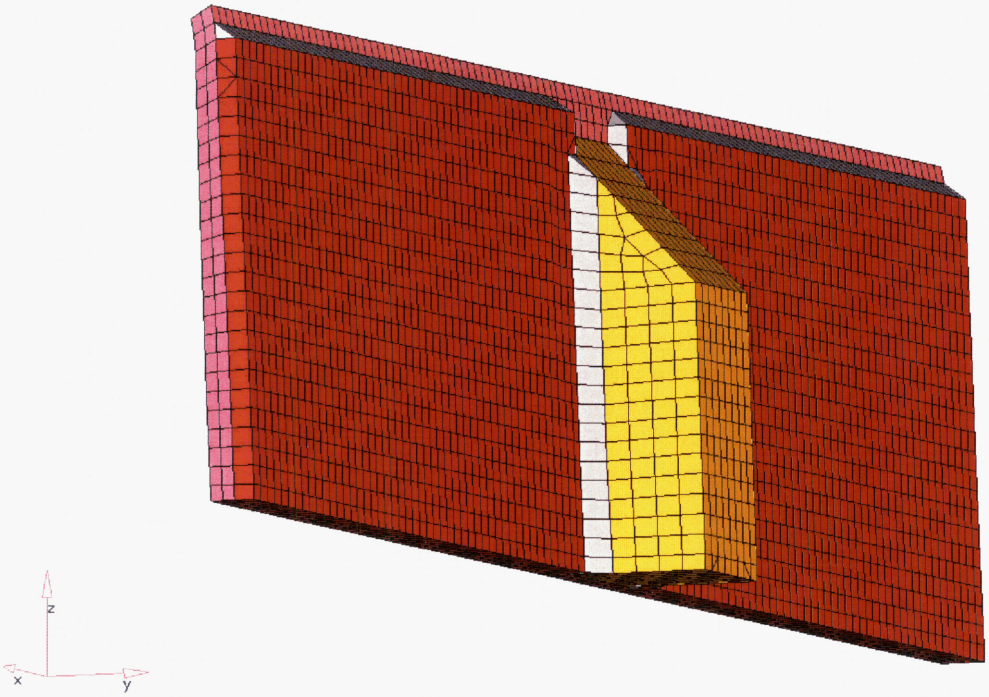

Figure 2-10b. Finite Element Model of the Drip Shield Corner to Obtain Moment-Rotation Curve (Exterior View)

The Von Mises stress distributions for the drip shield corner are shown in Figures 2-11 and 2-12. Figure 2-11 shows the yielding of the Titanium Grade 7 plate at the inner surface of the drip shield plate with the widest region of plasticity along the bottom edge of the plate. Figure 2-12a shows the plate, including the bulkhead beam. A significant portion of the plasticity was located along the bottom of the bulkhead where the bulkhead flange intersects the Titanium Grade 7 plate. Similarly, Figure 2-12b shows the plate with the support beam (column), where almost the complete cross section of the Titanium Grade 24 support beam yielded along the bottom edge of the support beam. Taking into consideration the deformation responses of the Titanium Grade 7 plate, Titanium Grade 24 bulkhead and Titanium Grade 24 support beam, failure would most likely occur along the bottom portion of the joint. Specifically, the critical section controlling the load capacity would be located in the cross-section containing the Titanium Grade 24 support beam (column) and the Titanium Grade 7 plate.

The moment-rotation curves obtained from the drip shield corner model are presented in Figure 2-13 for a drip shield temperature of 150 °C [302 °F]. The correlation between the moment-rotation relationship and the Von Mises stresses indicated that the Titanium Grade 7 yielding causes negligible degradation of the initial (elastic) stiffness. Significant flattening of the slope was only noticeable after yielding of Titanium Grade 24. Also, the ultimate moment of the drip shield corner model was controlled by the moment capacity of the bottom section of the drip shield corner (i.e., the top support beam section).

2.3.2.2 Drip Shield Support Beam

Two analyses utilizing the detailed drip shield finite element model (Section 2.2) were performed to obtain moment-rotation curves for critical sections of the drip shield walls. The deformation response of the support beams (columns) at the critical locations—0.6 m [1.97 ft] and 0.8 m [2.63 ft] (measured from the bottom)—were analyzed (Figure 2-14). The rotation was calculated based on deflection of the free end of the support beam (column) (Figure 2-14).

Figure 2-15 shows the obtained moment-rotation curves. In the support beam, the ultimate moments at 0.6 m [1.97 ft] and 0.8 m [2.63 ft] are 69 KN-m [50.9 k-ft] and 77 KN-m [56.8 k-ft], respectively. For both cases, the first yield of Titanium Grade 7 occurred at an approximate moment of 29 KN-m [21.4 k-ft], while the first yield of the Titanium Grade 24 occurred at approximately 46 KN-m [34 k-ft]. The moment curve was basically linear after the yielding of Titanium Grade 7. The ultimate moment was 1.5 to 1.7 times the moment at the first yield of Titanium Grade 24.

2.3.3 Drip Shield Finite Element Models Used to Validate the Drip Shield Frame Model

The structural response of the detailed finite element model (Figure 2-3) was obtained using specific system parameters and loading conditions. These results are used in Chapter 3 to verify the accuracy of the drip shield frame results. The loading pressures for this analysis were monotonically increased until drip shield structural instability occurs. The lateral-to-vertical pressure loading ratio is P_h/P_v = 0.45, see Figure 2-4.

The first yield of Titanium Grade 24 occurs at a P_v of 249 KPa [36 psi], it was located at the bottom part of the drip shield column frame (Figure 2-16), and became the critical section at

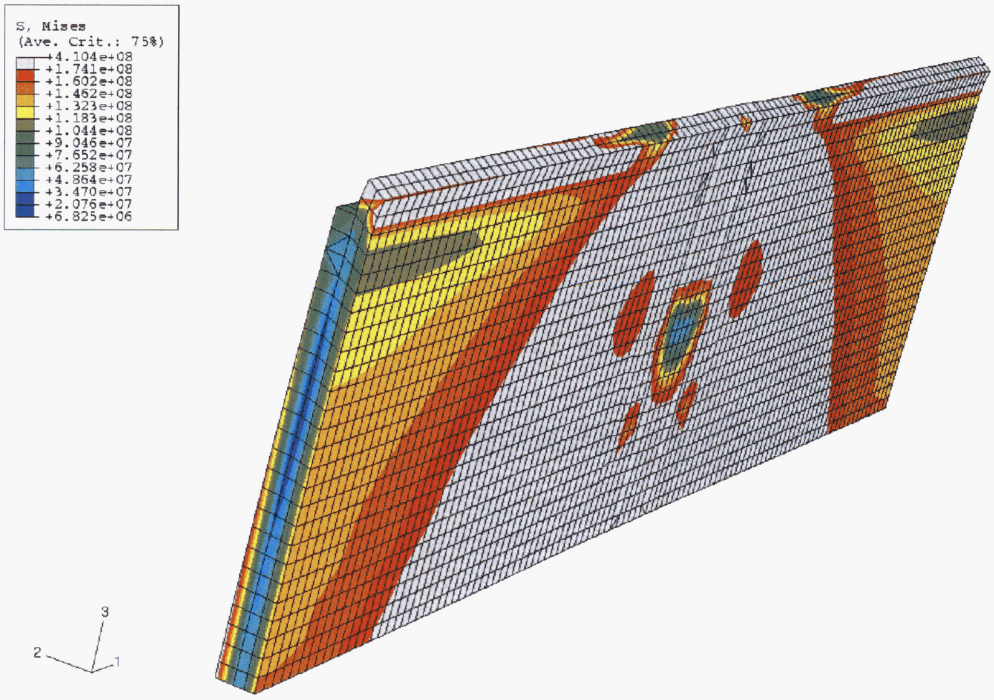

Figure 2-11. Moment-Rotation Titanium Grade 7 Yield Stress at Failure (Internal View)

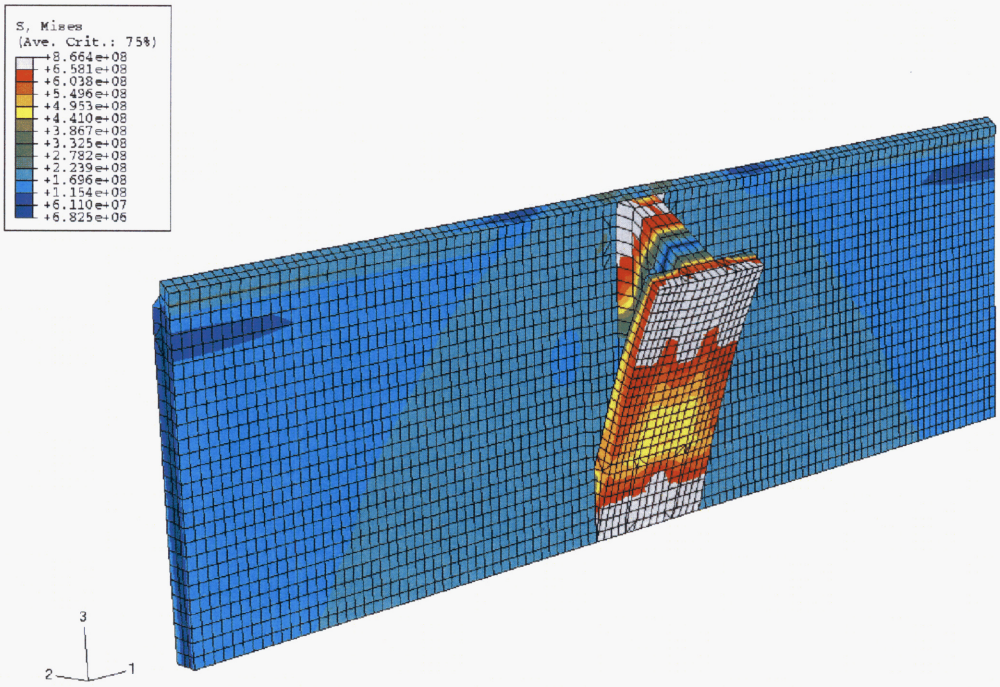

Figure 2-12a. Moment-Rotation Titanium Grade 24 Yield Stress at Failure (Internal View)

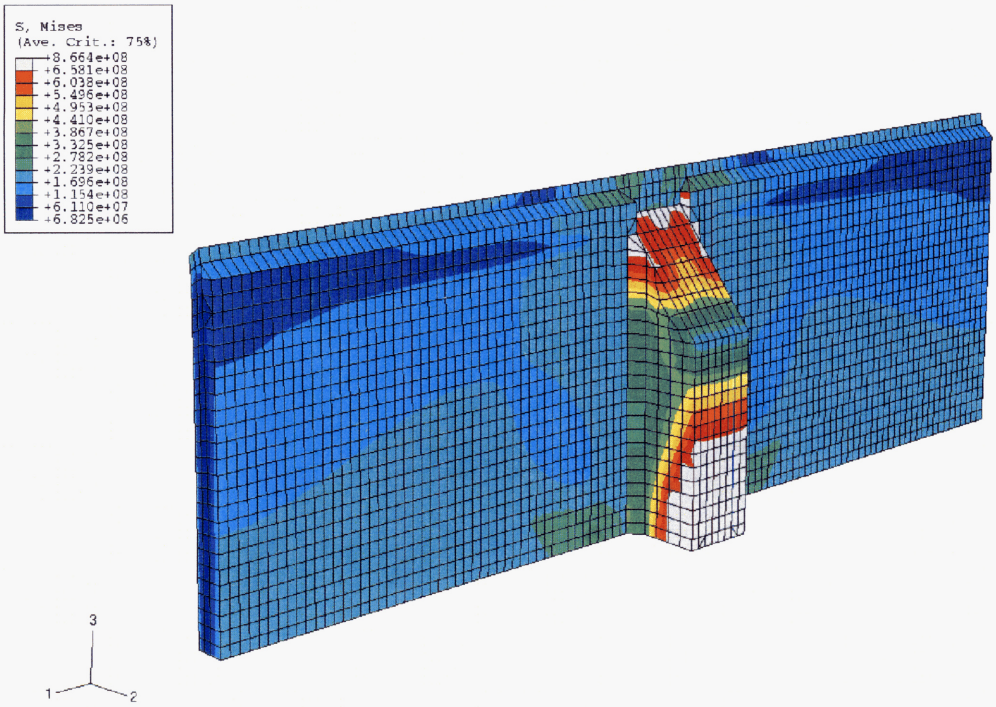

Figure 2-12b. Moment-Rotation Titanium Grade 24 Yield Stress at Failure (External View)

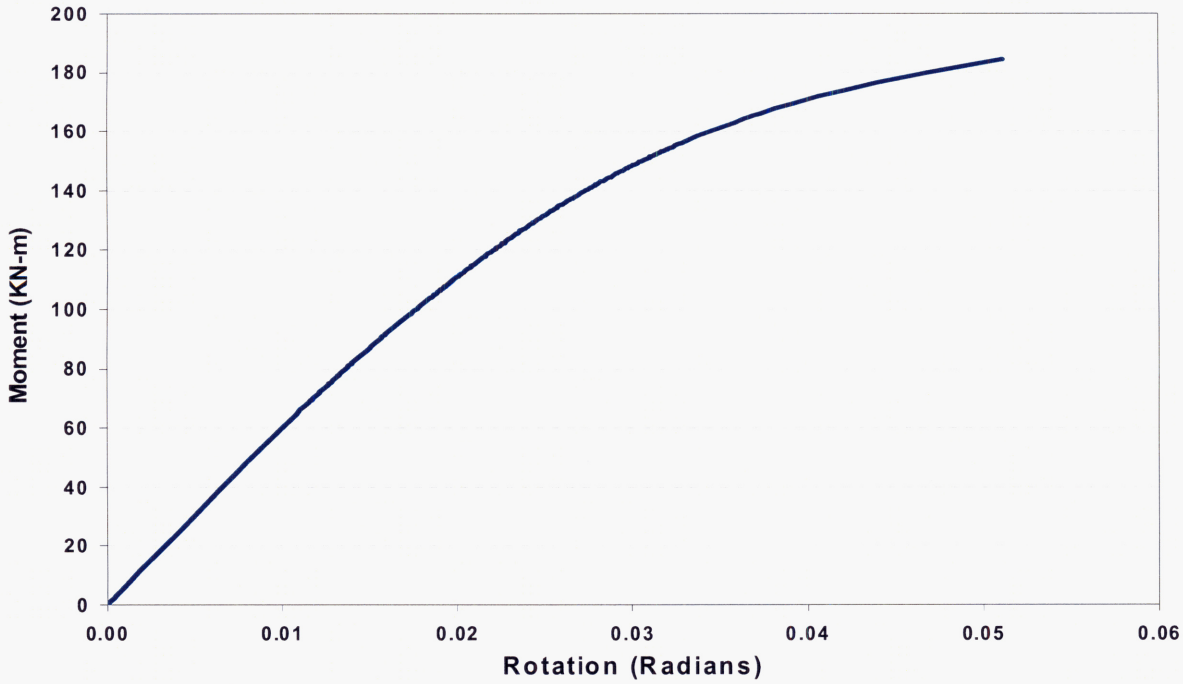

Figure 2-13. Moment-Rotation Curve for Drip Shield Corner

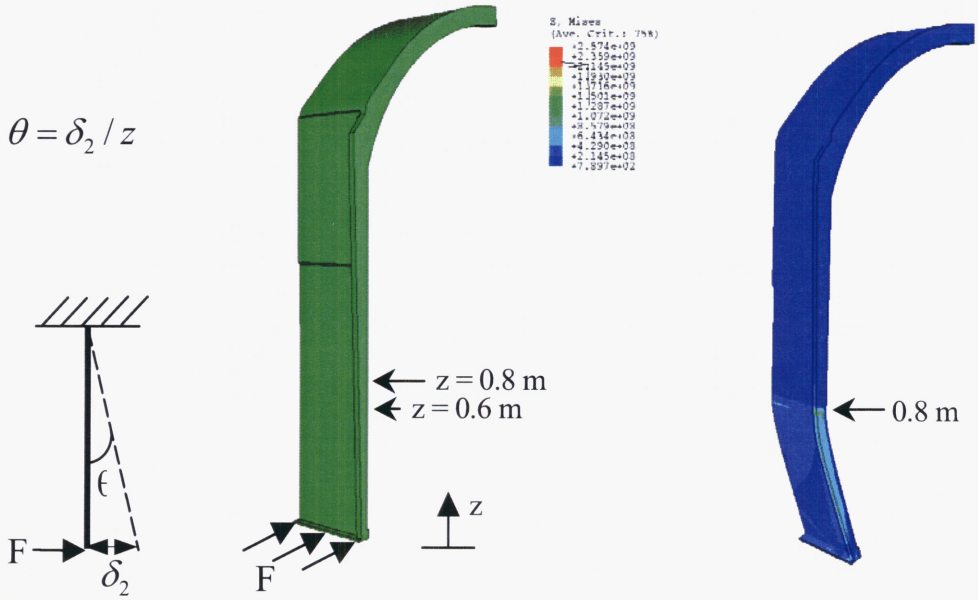

Figure 2-14. Analysis of Titanium Grade 24 Support Beam

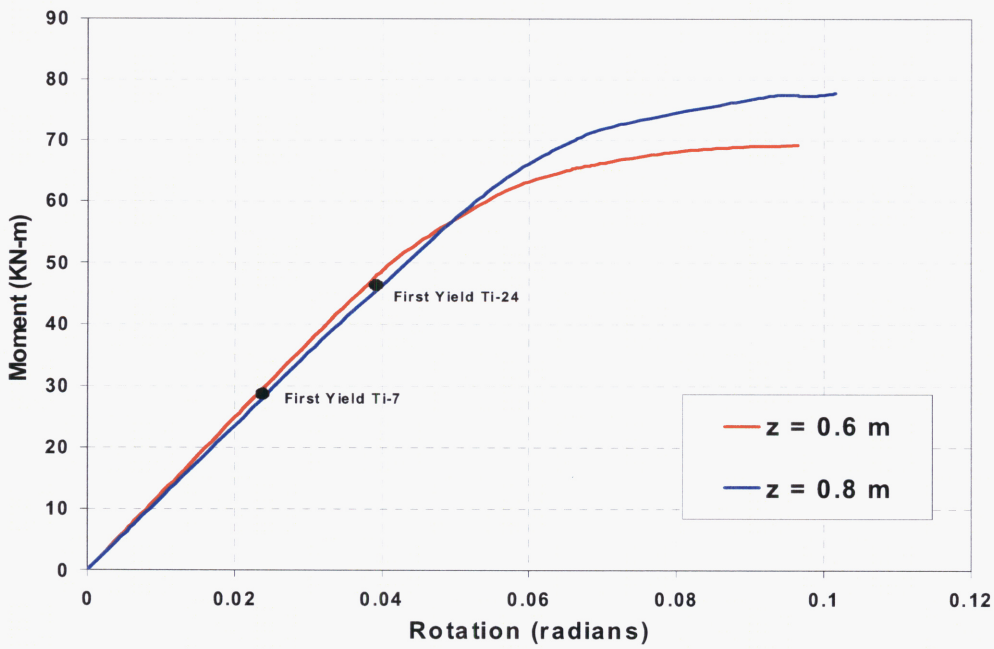

Figure 2-15. Moment-Rotation Response at the Support Beam from Finite Element Model

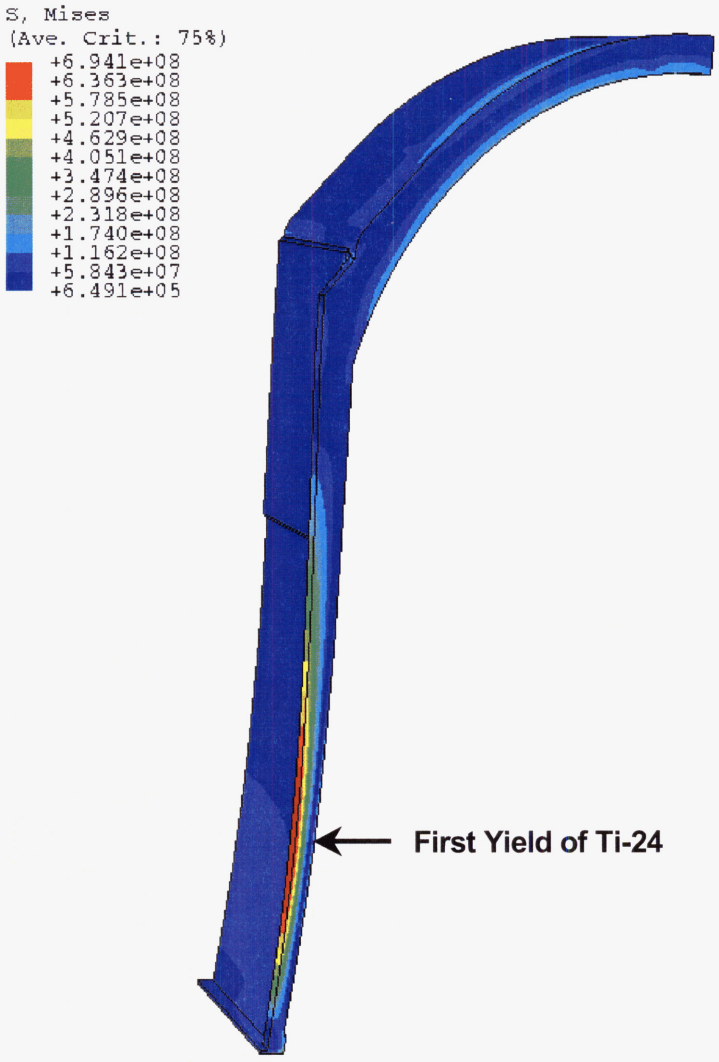

Figure 2-16. Drip Shield Von Mises Stress Distribution at Titanium Grade 24 First Yield

which failure of the drip shield occurred (Figure 2-17). The final collapse load occurred at a normal pressure P_v of 287 KPa [42 psi].

This particular drip shield finite element model analysis is discussed further in Chapter 3 with regards to the verification of the drip shield SAP2000 frame model.

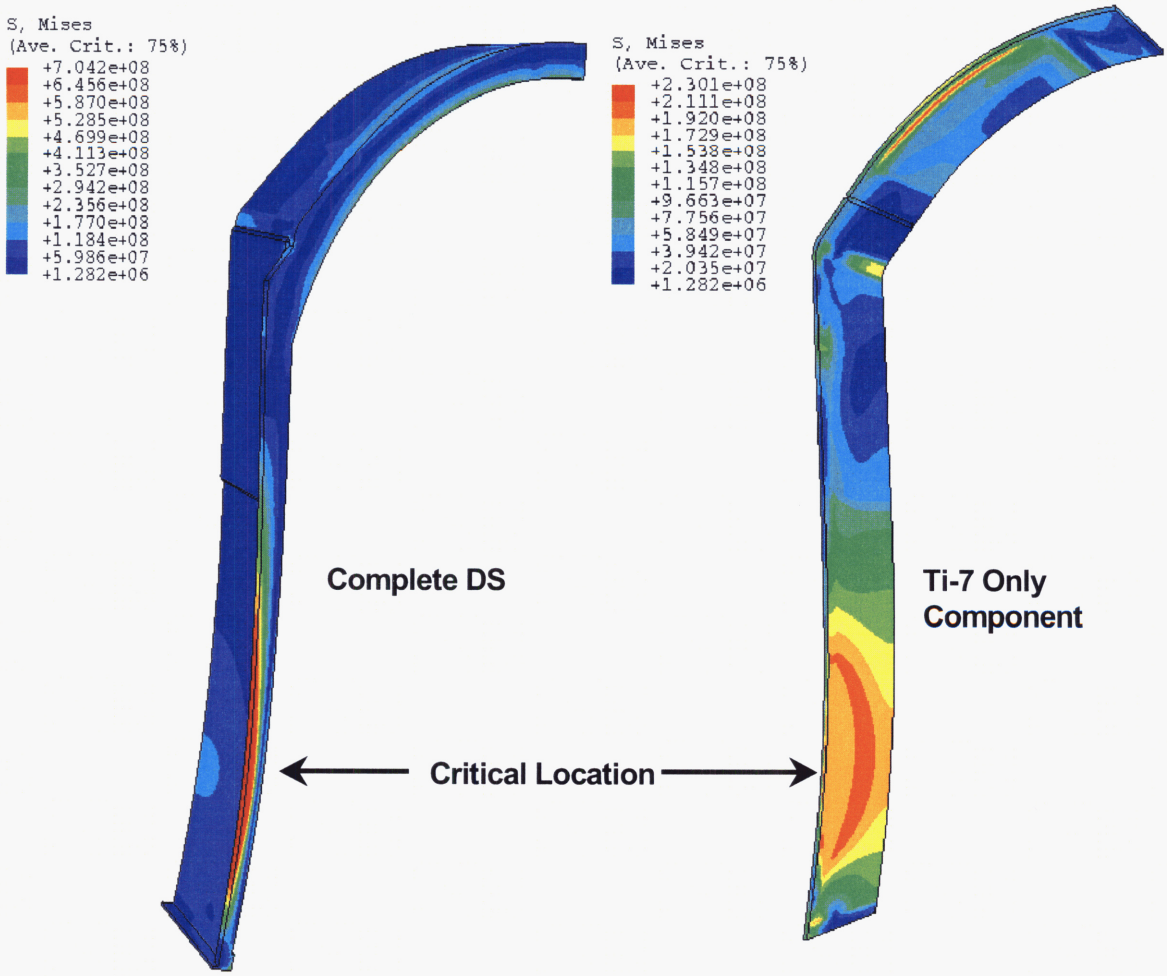

Figure 2-17. Drip Shield Von Mises Stress Distribution at Failure